Master thesis in Physical Oceanography

A study of the renewal of bottom water in Hjeltefjorden using observational data and a σ-coordinate ocean model

Gina Sørensen Aksnes

June 1, 2006

Geophysical Institute
University of Bergen
Norway

Acknowledgements

I would like to thank my supervisor, Tore Furevik, for able guidance and helpful advice. I would also like to thank Jarle Berntsen for his support on numerical problems. Furthermore, I would like to thank Einar Nygård for providing the observational data from Hjeltefjorden. I would like to thank all my fellow students at the Geophysical Insitute for making my time here enjoyable. Finally, I would like to thank Helge for encouragement and for proofreading my thesis.

Gina Sørensen Aksnes
Bergen, June 2006

Contents

Chapter 1

Introduction

During the buildup of the pipeline paths from the oil and gas production platforms in the North Sea to Kollsnes gas processing plant and Mongstad refinery, current meters were placed along the paths. The pipeline paths went through Hjeltefjorden and Fensfjorden, as Kollsnes is located adjacent to Hjeltefjorden, and Mongstad adjacent to Fensfjorden. These current meters were equipped with instruments for measuring salinity, temperature and pressure. The data from these current meters have been made available for this project through the Norwegian Deepwater Program (NDP). Although the data previously have been used for engineering purposes, (Eidnes 1999), a proper analysis of all oceanographic aspects has not yet been accomplished. Indications of bottom water renewal became the start of this master thesis.

My master thesies will include analysis of the current measurements and hydrography from Hjeltefjorden, as well as a study of the prosesses that lead to renewal of bottom water in Hjeltefjorden basin, using Bergen Ocean Model (BOM).

Hjeltefjorden is a fjord in the western part of Norway in Hordaland county. The fjord is an important fairway to Bergen as it provides the deepest passage (170 m) to the city through Hjeltesund at the southwestern entrance to Byfjorden. Hjeltefjorden spans from the island of Fedje in the north to Byfjorden in the south. In the west the fjord is delimited by Øygarden and Sotra. In the east it is delimited by among others Radøy, Holsnøy, Herdla and Askøy.

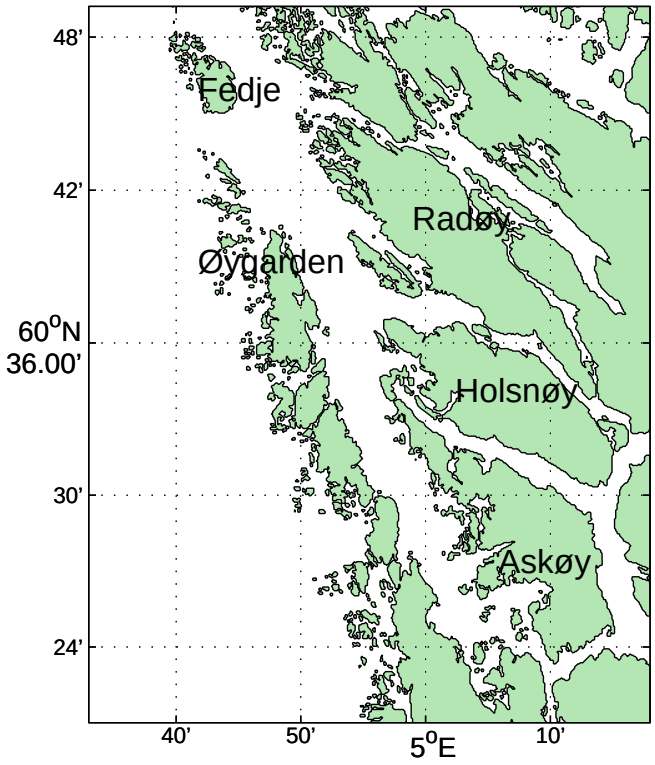

Figure 1.1: *Map over Hjeltefjorden and the delimiting islands.*

The current meters were located in the deepest parts of Hjeltefjorden (fig.1.2).

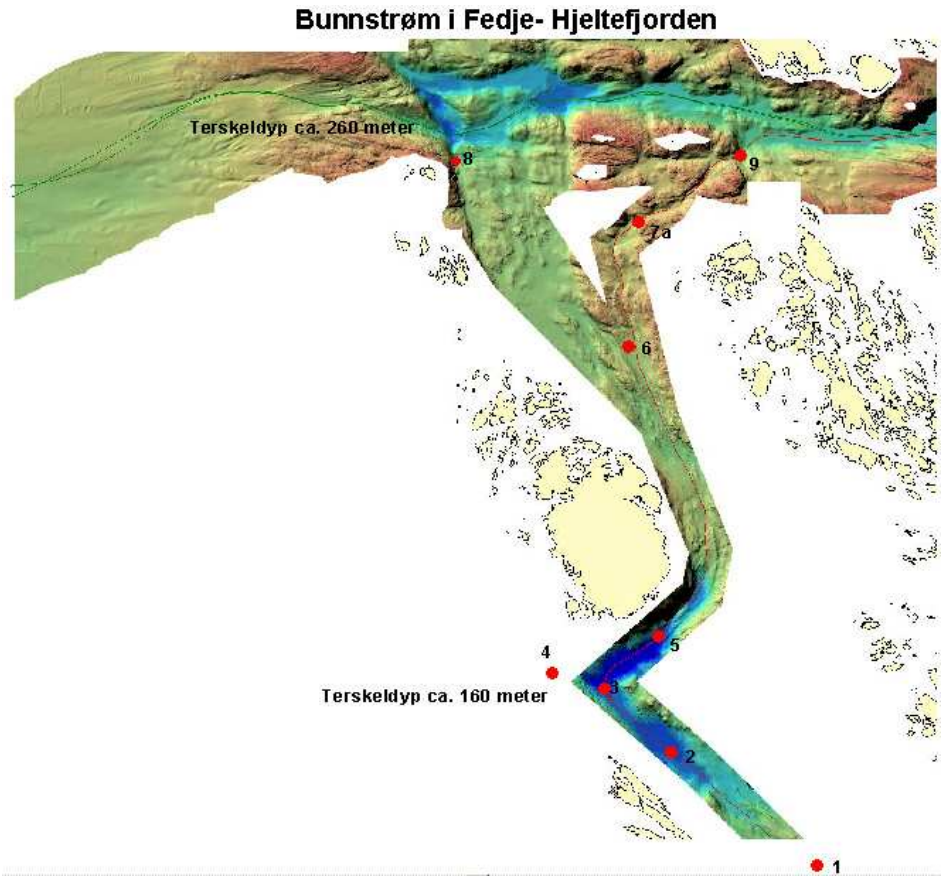

Figure 1.2: *Map over Hjeltefjorden showing the topography and the locations of the current meters. Map provided by NDP.*

There are few publications describing observations taken during events of basin water exchange. Helle (1978) presents current time series as well as hydrographic measurements during replacement of deep water in Byfjorden on the Norwegian west coast. He demonstrates that the exchange flow across the sill is basicly two layered, with a landward flow in the lower layer and an seaward flow in the upper layer, and the level of no-net motion located at mid-depth. Short period variations in the long-shore wind component are well reflected in the exchange flow. Wind speed extremes are followed one to two days later by corresponding extremes in the exchange flow, indicating the approximate response time for the upwelling process. Molvær (1980) describes observations of deep water renewal in Frierfjorden at the Norwegian Skagerrak coast. He concludes that the mainly wind induced density variations in the coastal water are very important for renewal of the intermediate and deep layer in the Frierfjord and the Langesundsfjord and that total phosphorous (TOTP) budgets may give valubale information on the extent of deep water renewals. Liungman, Rydberg & Göransson (2001) describe observations of deep water renewal in the Byfjord on the Swedish Skagerrak coast. By modeling the sill flow as well as the resulting dense bottom plume with various rates of entrainment, they found that sill mixing is relatively unimportant, but the entrainment increases the deep water inflow by a factor $2 - 4$. Entrainnment prolongs the time it takes for a complete renewal, and on moderate timescales yields lower post-renewal salinity and oxygen concentrations. This implies that entrainment during renewal may be as important as basin water diffusion in setting the timescale for forthcoming renewal events. Finaly Arneborg, Erlandsson, Liljebladh & Stigebrandt (2004) describe observations of deep water renewal in the basin of Gullmar Fjord on the Swedish Skagerrak coast. By using an autonomous profiling platform anchored in the middle of the fjord, they found that renewal starts with the passage of a gravity current front and continues with a steady thickening of the new, oxygen rich and low nitrate bottom layer and an associated lifting of the old, oxygen depleted, high nitrate bottom water. At the mouth of the fjord a three layer structure develops and renewal is driven by the density difference between the intermediate water inside and the new deep water outside the fjord. The fjords described in these articles have all relatively narrow and shallow mouths. Therefore the renewal of deep water continues for one week or longer in these fjords. Hjeltefjorden on the other hand has a relatively wide and deep mouth, and bottom water can therefore be renewed in the course of days or hours.

The data used in this thesis has to some extent been described in Eidnes (1999). The report presents a summary of the recorded current data as well as an harmonic analysis and directional extreme value analysis.

The main questions to be answered in this thesis are:

- Are periods of bottom water renewal recognizable in the observational data?
- What is the time needed to exchange the bottom water in Hjeltefjorden?
- Can periods of bottom water renewal be explained by atmospheric data?
- Can bottom water renewal be reproduced in a numerical model?
- How well do numerical model results compare to observational data?

This paper consists of seven chapters. In chapter 2 the observational data from Hjeltefjorden is presented, that is temperature and salinity measurements as well as current measurements. Further the observational data are used to calculate the propagation velocities of plumes of dense water intruding the fjord basin during periods of bottom water renewal. In chapter 3 observational wind data and NCEP Reanalysis data are used to test the hypothesis that offshore surface Ekman transports, and compensating deep onshore flows lifting dense water over the sill, are causing bottom water renewal. The Bergen Ocean Model (BOM) is presented in chapter 4 as well as the two different model setups used for this research. In chapter 5 the model results are presented and in chapter 6 the numerical model runs are first discussed seperately and then compared to the observational data. In chapter 7 the paper is summarized and concluded.

Chapter 2

Observational data from Hjeltefjorden

Hjeltefjorden is a sill fjord. The sill prevents outside water from intruding the fjord basin. For bottom water renewal to occur, water outside the fjord just below sill level has to be denser than the residing bottom water, and there must be some mechanism that can lift this water above sill level. If so, the dense water will spill over the sill and descend along the bottom of the fjord basin. The old basin water will be lifted to higher levels. With the intrusion of outside water, the state of the bottom water mass changes. The fjord becomes ventilated when typically cold, salty and oxygen rich water replaces the often oxygen depleted resident water.

The aim of this chapter is to give an oveview of the data that show changes in the state of the bottom water in Hjeltefjorden when the deep water is renewed.

Loc.	Position N	Position E	Water depth	Measur. depth	Instr.	Measurement period
1	60°41.500	04°48.717	$374m$	$371m$	$RCM-7$	980911 – 981007 981007 – 981214
2	60°43.550	04°44.700	$546m$	$543m$	$RCM-7$	980911 – 981007 981007 – 981208 981221 – 990228
3	60°44.283	04°43.267	$556m$	$553m$	$RCM-7$	980911 – 981007 981007 – 981212 981221 – 990224
4	60°44.533	04°41.917	$412m$	$39m$	$APCP$ $75kHz$	980911 – 981006 981008 – 981221
				$89m$		980911 – 981006 981008 – 981221
				$139m$		980911 – 981006 981008 – 981221
				$189m$		980911 – 981006 981008 – 981221
				$239m$		980911 – 981006 981008 – 981221
				$289m$		980911 – 981006 981008 – 981221
				$339m$		980911 – 981006 981008 – 981221
				$389m$		980911 – 981006 981007 – 981221
5	60°44.850	04°44.750	$497m$	$494m$	$RCM-7$	980911 – 980923 981007 – 981212 981221 – 990225
6	60°48.317	04°43.950	$307m$	$304m$	$RCM-7$	980911 – 981007 981007 – 981221 981221 – 990306
7	60°49.950	04°44.133	$261m$	$258m$	$RCM-7$	981007 – 981103
$7a$	60°49.710	04°43.750	$283m$	$280m$	$RCM-7$	981103 – 981221 981221 – 990225
8	60°50.917	04°40.567	$454m$	$451m$	$RCM-7$	980911 – 981007 981007 – 981218
9	60°50.700	04°46.680	$285m$	$282m$	$RCM-7$	981103 – 981221 981221 – 990226

Table 2.1: *Overview over the current meter data. The table gives the location of the current meters, the depth of the fjord where the current meters were deployed, at which depth the current meters were placed, instrument type and finally the measurement periods.*

2.1 Temperature and salinity measurements

The following plot shows how the salinity, temperature and density at the bottom of Hjeltefjorden evolves over a time period of six months during the winter season. The salinity and temperature are measured, whereas the density is derived from measured salinity, temperature and pressure using the UNESCO 1983 polynomial fit (Fofonoff & Millard 1983).

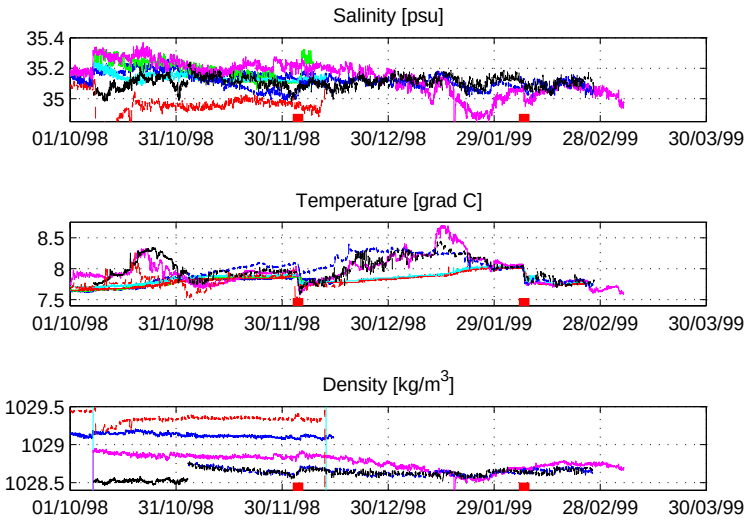

Figure 2.1: *Salinity, temperature and density at the bottom of Hjeltefjorden from the 1st of October 1998 to the 30th of March 1999. The two periods that will be focused on, are marked as red bars on the time axis.*

At two different time periods, sudden changes in the properties of the bottom water were especially clear. The periods are marked in red in figure 2.1. Such changes in the bottom water properties are indications of intrusion of new water masses and bottom water renewal. The two periods will throughout the text be referred to as period 1 and period 2.

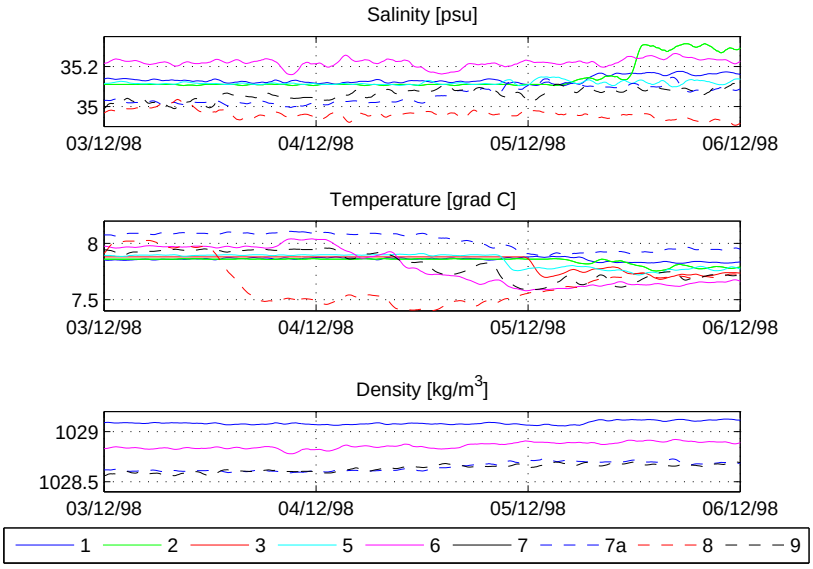

Figure 2.2: *Salinity, temperature and density at the bottom of Hjeltefjorden from the 3rd to the 6th of December 1998, period 1. The legend refers to the locations given in table 2.1.*

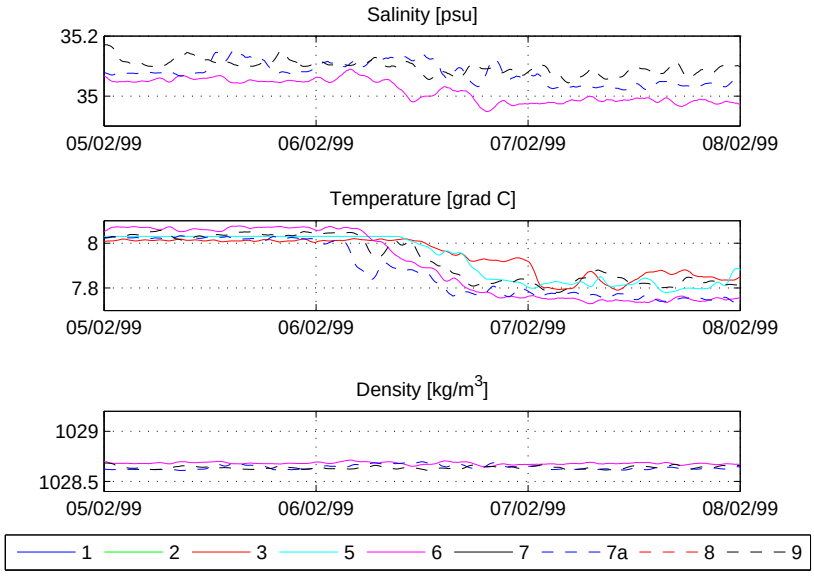

Figure 2.3: *Salinity, temperature and density at the bottom of Hjeltefjorden from the 5th to the 8th of February 1999, period 2. The legend refers to the locations given in table 2.1.*

2.2 Current meter data

As mentioned in the introduction, current meter moorings were placed along the pipeline paths from the North Sea to terminals at Mongstad and Kollsnes during the buildup of these. The data retreived from the current meters include current velocity and direction, as well as salinity, temperature and pressure. The data have kindly been made available through the Norwegian Deepwater Program (NDP).

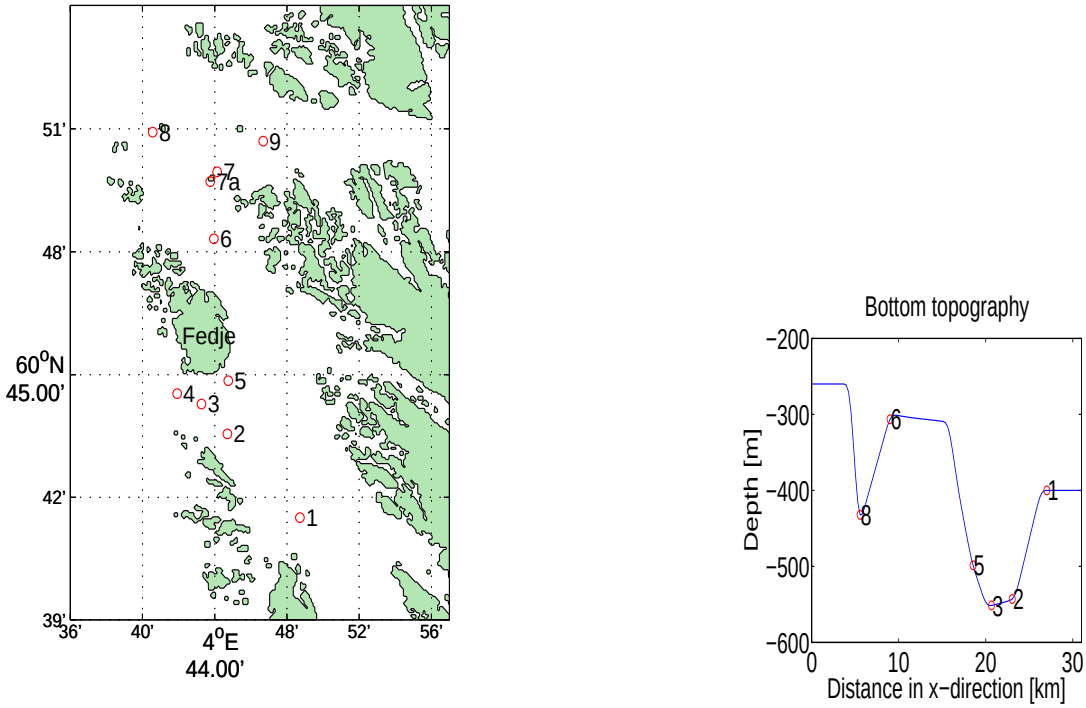

Figure 2.4: *Map of Hjeltefjorden (left), and a schematic long-fjord plot of the bottom topography in the deepest channel of the fjord basin (right). The current meter locations are marked with red dots.*

Station 8 is located just behind the sill at the entrance of the fjord (fig.2.4). Given that the intrusion of cold and dense Atlantic water begins at station 8, the expected direction of the plume of dense water will be through the deepest path in the fjord basin. This is where the current meters are located. The plume of dense water is expected to first reach station 7a/7 then station 6, station 5, station 3, station 2 and at last station 1. Station 9 as well as station 4 are located off the chosen path through Hjeltefjorden, and will not be used in this study.

With the incoming plume of dense Atlantic water one would expect an increase in the current velocity at the bottom of the fjord. The expected direction of the current would be southward. This can indeed be seen (fig.2.5, fig.2.6 and fig.2.7).

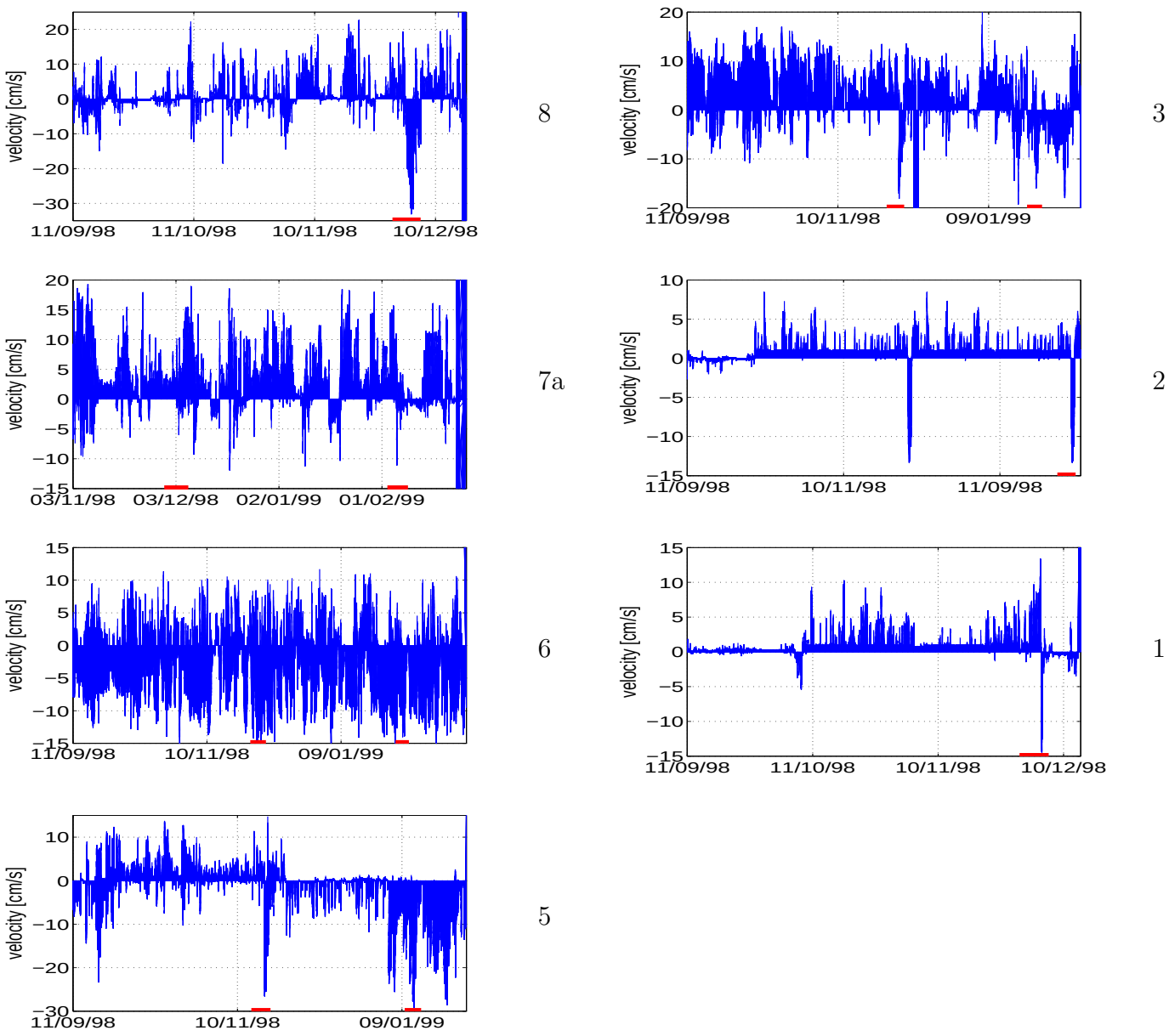

Figure 2.5: *The current velocity and direction at the different stations for the entire measuring periods. Period 1 and period 2 are indicated with red bars along the time axis.*

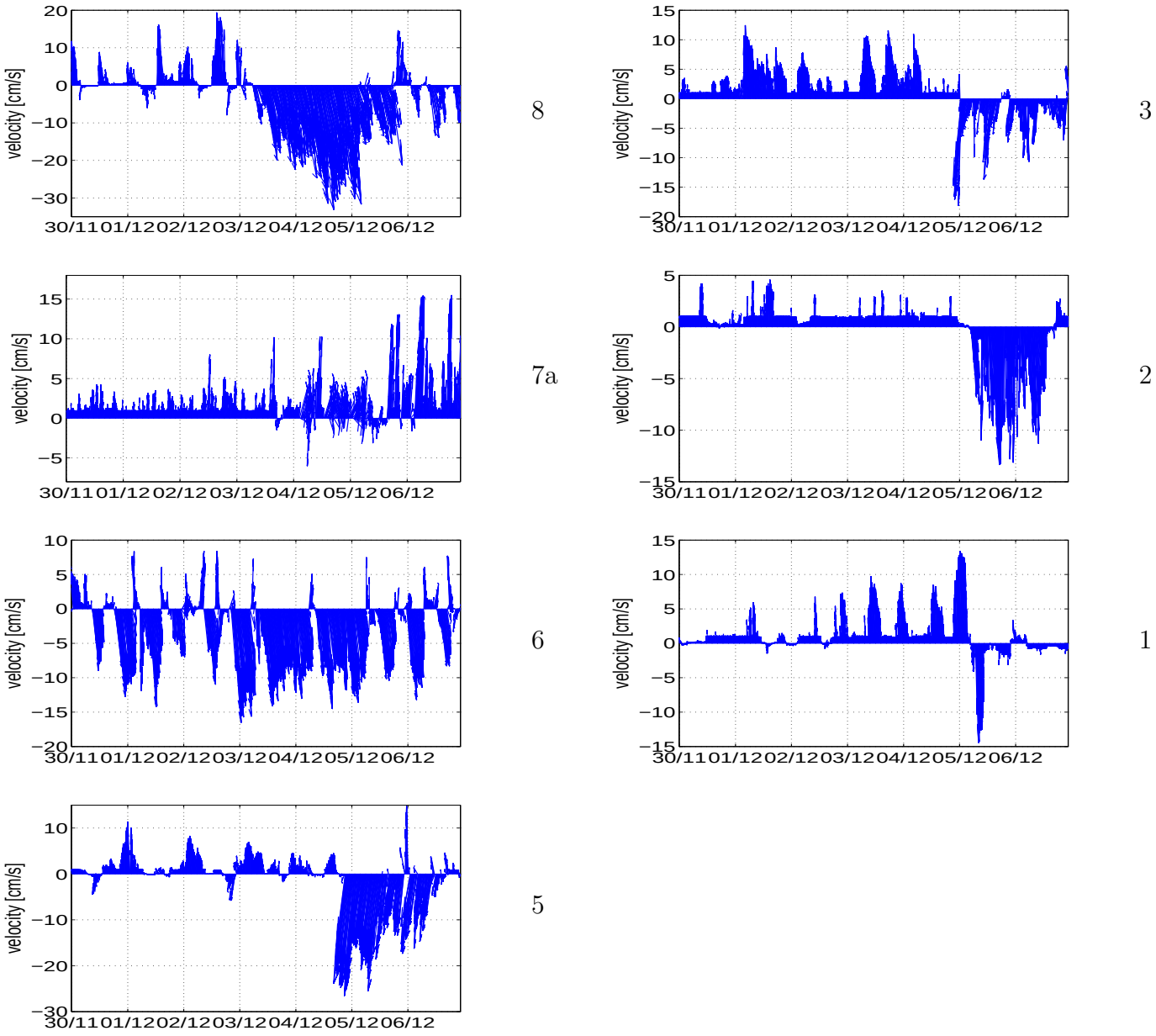

Figure 2.6: *The current velocity and direction at the different stations from the 30th of November to the 6th of December 1998, period 1.*

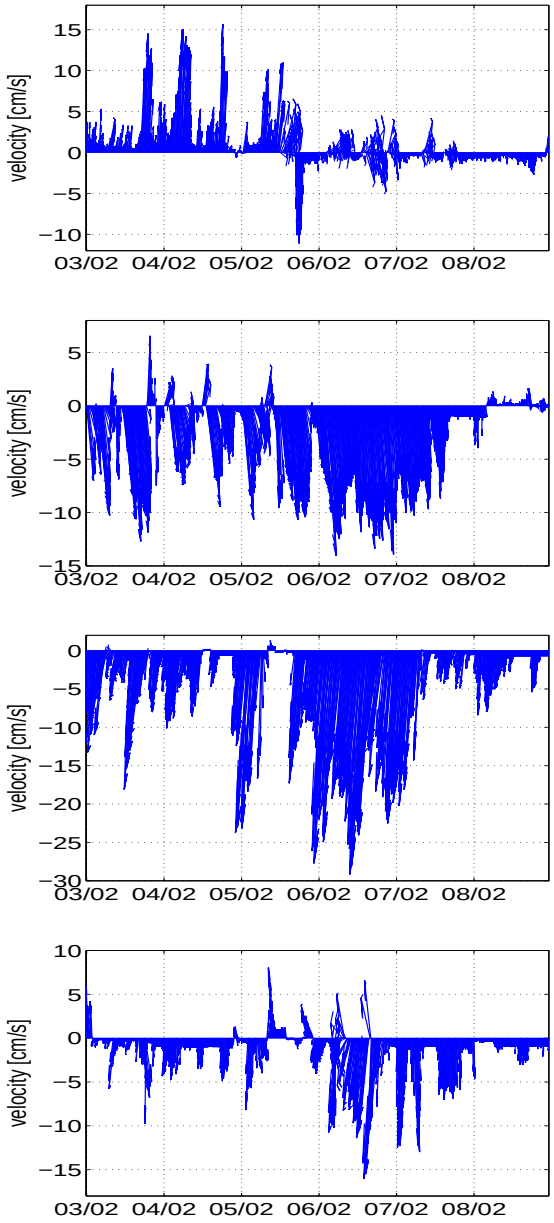

Figure 2.7: *The current velocity and direction at the different stations from the 3rd of February to the 8th of February 1999, period 2.*

2.3 Propagation velocities

The velocities of the plume fronts, c, can be derived from measuring the distance between two stations, s, as well as the time it takes for the plume to travel between the stations, t.

$$c = \frac{s}{t} \tag{2.1}$$

The distance is calculated along the deepest channel in the fjord, (fig.1.2), but the topography is not considered.

From looking at figure 2.2 and using equation 2.1, we get the approximate plume velocites shown in the following table (2.2).

Location	Distance [km]	Δt [h]	Velocity of the plume [cm/s]
station $8-6$	5.7	13.4	12
station $6-5$	7.1	16.2	12
station $5-3$	1.7	3.2	15
station $3-2$	3.3	3.7	25
station $2-1$	5.3	2.8	53

Table 2.2: *Velocity of the plume of bottom water propagating through the fjord in period 1 (fig.2.2).*

Following the same procedure as above, figure 2.3 gives the phase velocities shown in the next table (2.3).

Location	Distance [km]	Δt [h]	Velocity of the plume [cm/s]
station $7a-6$	2.6	4.6	16
station $6-5$	7.1	11.5	17
station $5-3$	1.7	1.8	26

Table 2.3: *Velocity of the plume of bottom water propagating through the fjord in period 2 (fig.2.3).*

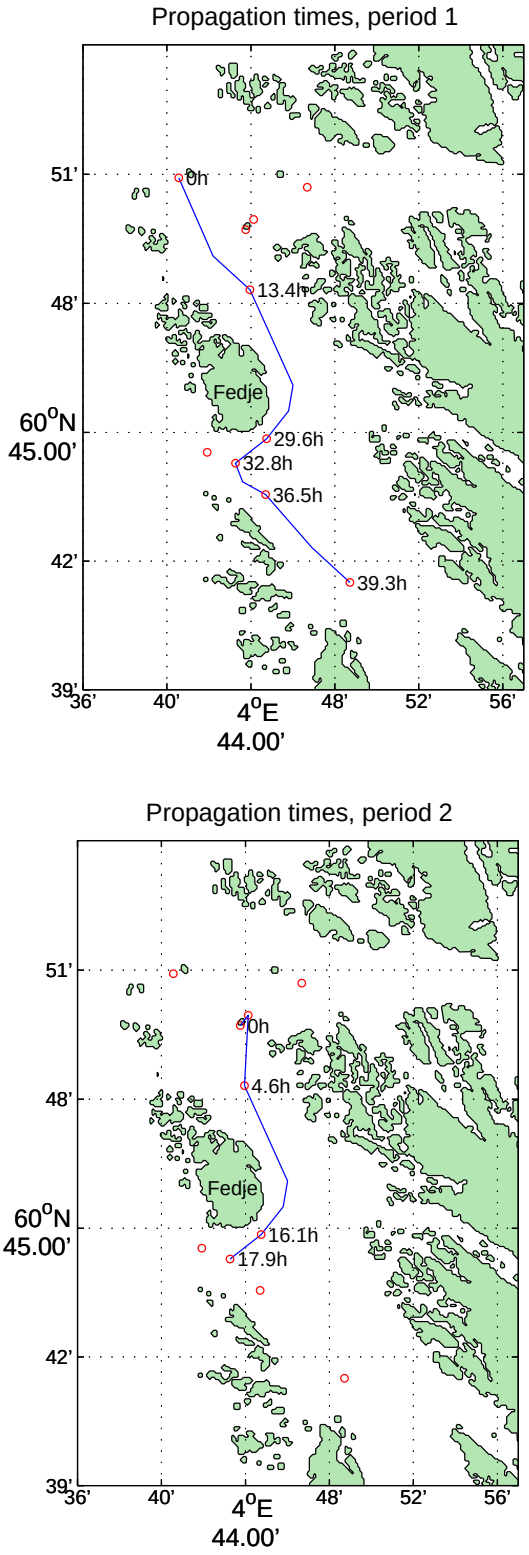

Figure 2.8: *Map over Hjeltefjorden and the locations of the current meters. Marked in are the paths wich the plumes of new bottom water travelled as well as the time it took to propagate from one station to the next. At top the path form the 3rd to the 6th of December 1998 (period 1), and at bottom the path from the 5th to the 8th of February 1999 (period 2).*

2.4 Discussion

This discussion is based on the assumption that the two periods of sudden changes in the properties of the bottom water (fig.2.1) originates from outside the fjord, and is not the result of an internal displacement of water masses. This assuption is probable considering that the temperarure drop reaches $0.5°C$, and that the change is visible at all of the stations.

The intrusion of new water masses in Hjeltefjorden is particulary evident in the temperature plot. In period 1 (fig.2.2) the temperature drop reach $0.5°C$ at some of the stations. In period 2 (fig.2.3) the largest drop in temperature is $0.3°C$. Because of the small differences in the salinity in Hjeltefjorden and the Atlantic water outside, the salinity remains almost unchanged. As the Atlantic water that intrudes the fjord basin in period 1 and period 2 is colder, it is heavier than the residing bottom water.

It is possible to follow the plumes of water as they progress through the fjord. For period 1 (fig.2.2) the temperature drop is first evident at station 8, after follows station 6, station 5, station 3, station 2 and station 1. For period 2 (fig.2.3) the temperature drop is first evident at station 7a, then station 6, station 5 and station 3. This coincides with the signals in the current velocity and direction (fig.2.6 and 2.7). The plumes of cold and dense water are thus moving according to our hypothesis.

Around the 3rd, 4th and 5th of December, the current velocity is increasing (fig.2.6). The direction of the current is changing from station to station. This is expected because of the alignment of the deep channel in the fjord that the current meters are placed in. The direction of the current will shift as it passes through the channel. But at most stations the main direction of the currents are southward. The increase in velocity is first visible at station 8, then station 6, station 5, station 3, station 2 and at last station 1. At station 7a it is hard to see changes in the velocity.

Around the 5th and 6th of February the current velocity is increasing (fig.2.7). The increase can be seen at station 6, station 5 and station 3. It is first visible at station 6, then at station 5 and at last at station 3 wich is expected based on the assumption that the signal originates from the entrance of the fjord.

The Rossby Radius of Deformation, R_D, is the horizontal length scale at which rotation effects become as important as buoyancy effects (Gill 1982). For a two layer fjord like Hjeltefjorden (see fig.2.9), the baroclinic Rossby radius is given by:

$$R_D = \frac{\sqrt{g'H}}{f}, \tag{2.2}$$

$$g' = \frac{\rho_2 - \rho_1}{\rho_2} \times g, \tag{2.3}$$

Here H is the depth of the upper layer, ρ_1 and ρ_2 are the density of respectively the upper and the lower layer, g is the gravity acceleration and f is the Coriolis parameter.

Using density measurements from a cruise on Hjeltefjorden with R/V Haakon Mosby (fig.2.9) we estimate $\rho_1 = 1025.25 kg/m^3$, $\rho_2 = 1027.25 kg/m^3$, $H = 100m$ and $f = 10^{-4} s^{-1}$. This gives a typical Rossby radius for Hjeltefjorden,

$$R_D = 14km \tag{2.4}$$

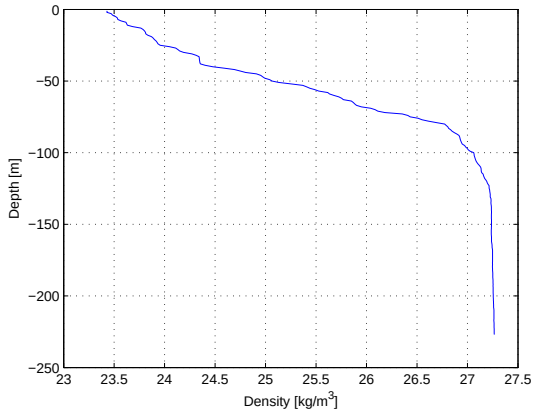

Figure 2.9: *Measured density in a CTD-profile taken in Hjeltefjorden at* $60°33'N$ *and* $4°54'E$ *the 14th of October 1998.*

This means that watermasses in motion can be influenced by the earths rotation in some parts of Hjeltefjorden, where the width of the fjord is sufficently large.

This may be one of the reasons why there is no increase in current velocity at station 7a in period 1. The plume of dense water may become deflected to the right by the earths rotation. If so, an increase in velocity would have been visible at the western side of the channel, but not in the middle where the current meters are located. However, the incoming new water masses is evident in the hydrological measurement. This may be a result of mixing between the incoming plume of dense water and the resident deep water.

Looking at the propagation velocities calculated for the incoming plume of dense water, the increase in velocity as it progresses through the fjord can be partly explained as a response to the bottom topography.

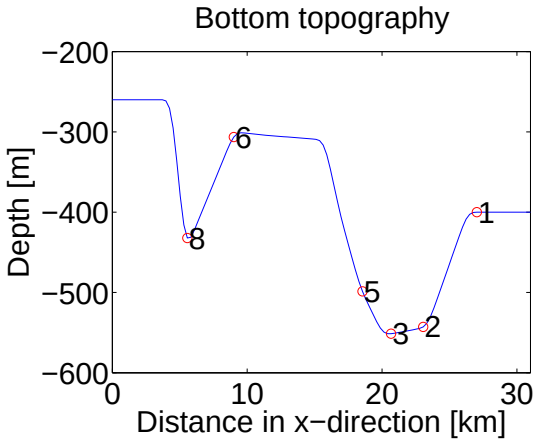

Figure 2.10: *A long-fjord plot of the bottom topography in the deepest channel of the fjord basin.*

Between station 8 and station 6 there is an upward slope. Thus the local basin must be filled before the dense water can reach station 6, and we get low velocity. Between station 6 and station 5 there is a downward slope and as expected the velocity increases due to gravity pull. From station 5 to station 3 the downward slope continiues and the velocity increases even more. Between station 3 and station 2 the topography is practically flat with a slight upward slope and the velocity increases again. This is an effect of inertia. The plume of water has generated velocity down the hill from station 6 to station 3 and will not stop abruptly. But this will not explain why the velocity increases from station 2 to station 1 even though the topography is continiously upward sloping.

Another factor that can affect the velocity of the plume, is the tidal currents. The semidiurnal tides has a period of 12 hours and 25 minutes. This means that the tidal currents use 12 hours and 25 minutes progressing into the fjord, and out again. If the plume of dense water travels with the tidal currents, its velocity may increase, and if the plume travels against the tidal currents, its velocity may decrease. Travelling from station 8 to station 6, the plume uses $13.4h$. The plume reaches station 6 after $29.6h$, station 3 after $32.8h$, station 2 after $36.5h$, and finally station 1 after $39.3h$. Given that the plume entered the fjord basin as a tidal period started, the plume will experience three full tidal periods and the start of a fourth as it progresses through Hjeltefjorden. Since the travelling time from station 8 to station 6, is about one full tidal period, the plume travels both with, and against the tidal currents, and combined the velocity of the plume will not be affected. From station 6 to station 5 the plume uses $16.2h$, that is one full tidal period and four hours. Combined the plume will travel with the tidal currents more than against, and the velocity of the plume may increase. From station 5 to station 3 the plume travels both with and against the tidal currents and its velocity

may not be affected. From station 3 to station 2, the plume will travel against the tidal currents, and the velocity may decrease. And finally from station 2 to station 1 the plume travels with the tidal currents at the start of the fourth tidal period, and the velocity may increase. This may be why the velocity of the plume increases between station 2 and station 1.

Chapter 3

Atmospheric data

In sill fjords, renewal of bottom water usually occurs when dense water outside the fjord is lifted above sill level and can flow in and replace the residing bottom water. Northerly winds along the west coast of Norway induce coastal divergence in Ekman transports and upwelling of denser water, which can spill over the sill and decend along the bottom of the fjord basin. The old basin water will be pushed away and lifted to higher levels. Bottom water renewal in a fjord basin is associated with seasonal changes of the density structure offshore. In Norwegian fjords such changes are coupled to the monsoonal nature of the wind field, being predominantly northerly in the summer and southerly in the winter (Gade & Edwards 1980). This means that wind induced renewal of bottom water is more frequent in the summer than in the winter. But also during the winter season, bottom water renewal occurs. The phenomenon is usually linked to a change in the wind field from southerly to northerly associated with a low pressure system over Norway. The aim of this chapter will be to explore the periodes of bottom water renewal using observed wind data from the Norwegian Meteorological Institute (http://www.met.no) and NCEP Reanalysis data provided by the NOAA-CIRES Climate Diagnostics Center, Boulder, Colorado, USA, from their Web site at http://www.cdc.noaa.gov/.

3.1 Observational data

Time series of wind data from a measurement station called Hellisøy Fyr just off the southern coast of Fedje in Hjeltefjorden (map fig.2.4), was downloaded from the eklima database of the Norwegian Meteorological Institute at http://eklima.met.no/. The data contains wind velocity and direction, observed every sixth hour $10m$ above the sea surface.

Below, the wind data is plotted (fig.3.1). We give an overview of the wind patterns from the 1st of September 1998 to the 31st of March 1999. Next we focus on the two periods with bottom water renewal, period 1 and period 2.

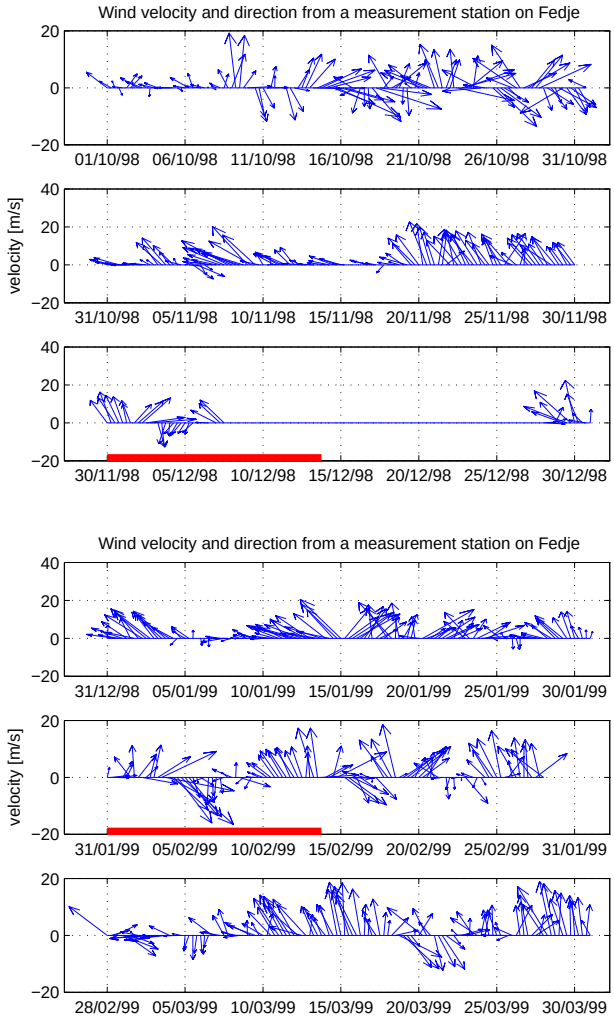

Figure 3.1: *Observed wind velocity and direction from the 1th of September 1998 to the 30th of March 1999. Each plot containing one month of data.*

In September the direction of the wind is constantly changing with no clear pattern, whereas in October the direction is predominately southeasterly. December begins with southerly wind, but shortly before period 1, the direction of the wind shifts to northeasterly. There are no data for the rest of December until the last few days where the winds are southerly.

Throughout January the prevailing wind direction is southerly. During the first half of January the direction is mainly southeasterly, whereas half way through the month the wind direction shifts to southwesterly. In February the wind direction is mainly southeasterly, but shortly before period 2, the direction shifts to northwesterly. Through March the direction of the wind is predominately southeasterly.

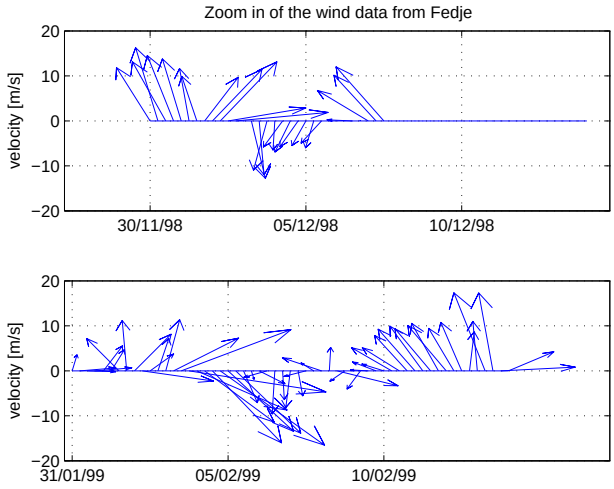

Figure 3.2: *Zoom-in over the observed wind data from the two periods with bottom water renewal.*

The direction of the measured wind shifts from southerly to northerly at the days of bottom water renewal, and shifts back afterwards (fig.3.2). This is consistent with the assuptions that a change to northerly winds can give a deep inflow.

3.2 NCEP Reanalysis data

At large scales the winds are in geostrophic balance, that is, they tend to be parallel to the isobars, leaving low pressure to the left and high pressure to the right in the Northern Hemisphere. That is, the wind flows counterclockwise around a low pressure system. Furthermore, at all latitudes the speed of the wind tends to be inversely proportional to the spacing of the isobars (Wallace & Hobbs 1977).

As explained earlier in this chapter, northerly winds along the west coast of Norway induce uppwelling of denser water to the sill depth, leading to renewal of bottom water in sill fjords. According to theory it is expected to find a low pressure over Norway at periods of bottom water renewal, as such a low pressure system would generate northerly winds at the coast of Norway.

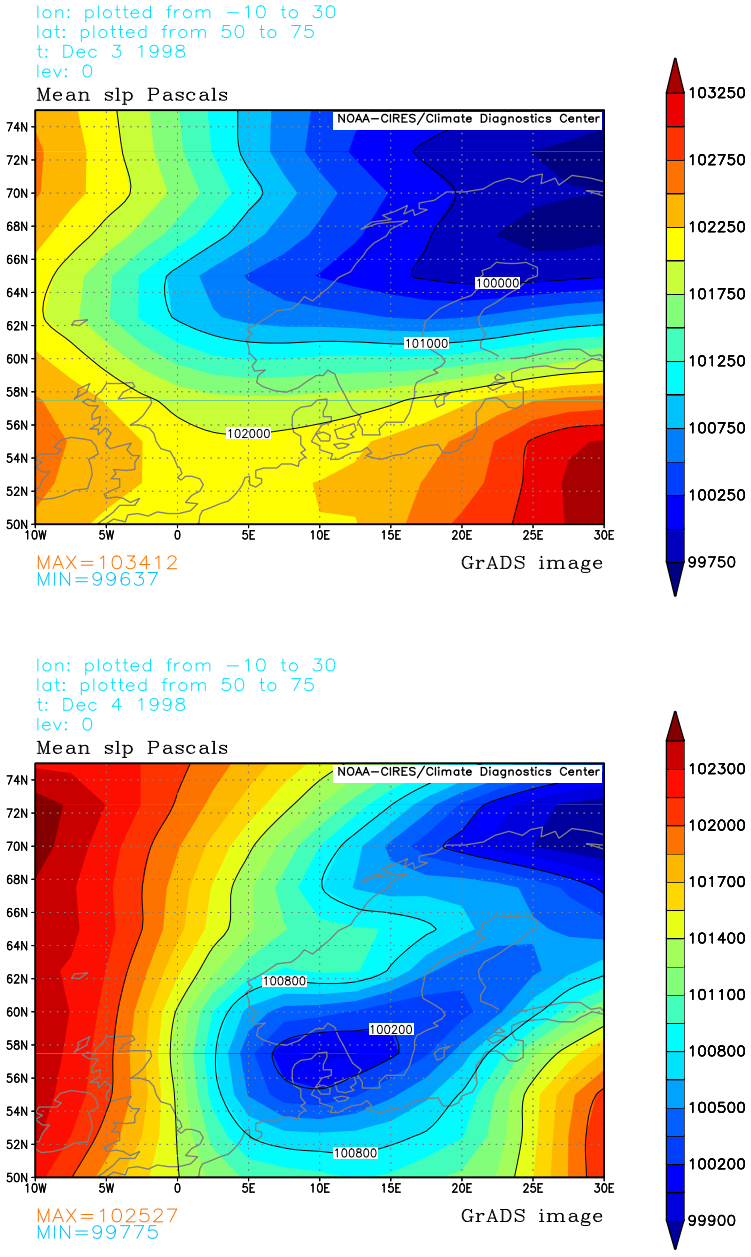

Figure 3.3: *Sea level pressure over Norway at the 3rd and the 4th of December 1998 in period 1.*

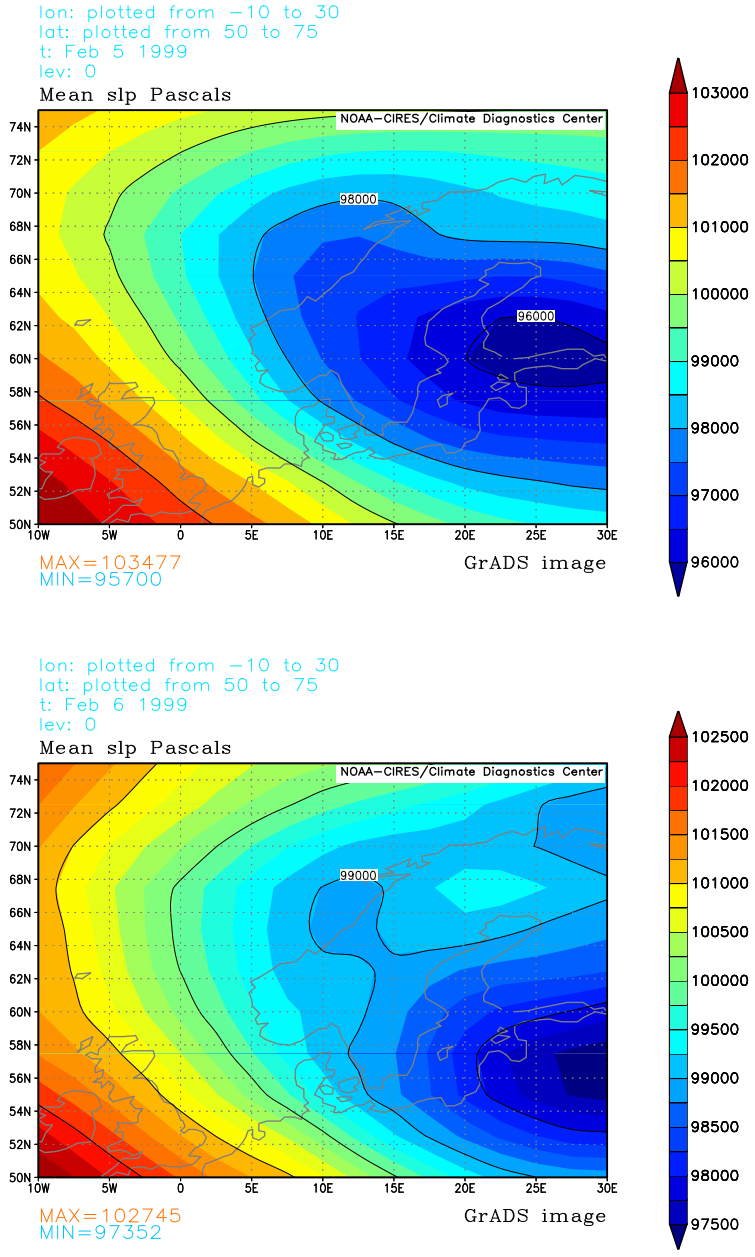

Figure 3.4: *ASea level pressure over Norway the 5th and the 6th of February 1999 in period 2.*

Figure 3.3 and 3.4 shows contour plots of the sea level pressure over Scandinavia for the two periods with bottom water renewal. The plots are based on the NCEP reanalysis data. From both periods one can see low pressure systems over Norway. At the west coast of Norway these will cause northerly winds, which will lead to upwelling along the coast of Norway, consistent with our hypothesis.

Chapter 4

Bergen Ocean Model (BOM)

A numerical ocean model was used to study a plume of dense water as it progresses through Hjeltefjorden. This phenomenon is related to the renewal of bottom water in the fjord. A σ-coordinate, or terrain following, model was chosen, as it allows a fine resolution of the bottom boundary layer.

The Bergen Ocean Model (BOM), is a σ-coordinate numerical ocean model developed at the Institute of Marine Research and the University of Bergen. It is described in Berntsen (2000). The variables are discretized using finite difference methods. The horizontal finite difference scheme is staggered using an Arakawa C-grid (Mesinger & Arakawa 1976). The model is mode split similarly with the splitting described in Berntsen, Kowalik, Sælid & Sørli (1981).

4.1 The basic equations

For studying bottom water renewal in Hjeltefjorden, the coordinate system (x, z, t) was used, where x is the horizontal coordinate, z the verticale coordinate and t is time. Based on scaling analysis we neglected the effect of rotation and non-hydrostatic motion. These are plausible assumptions since this was a small scale study, both in time and space (Gill 1982). The basic equations in BOM are given below:

The continuity equation:

$$\frac{1}{\rho}\frac{D\rho}{Dt} + \frac{\partial U}{\partial x} + \frac{\partial W}{\partial z} = 0. \tag{4.1}$$

where ρ is the in situ density, U the horizontal velocity in x-direction and W the vertical velocity in the z-coordinate system.

For an incompressible ocean the continuity equation becomes:

$$\frac{\partial U}{\partial x} + \frac{\partial W}{\partial z} = 0. \tag{4.2}$$

The Reynolds momentum equations :

$$\frac{\partial U}{\partial t} + U\frac{\partial U}{\partial x} + W\frac{\partial U}{\partial z} = -\frac{1}{\rho_0}\frac{\partial P}{\partial x} + \frac{\partial}{\partial z}\left(K_M \frac{\partial U}{\partial z}\right) + F_x, \tag{4.3}$$

$$\rho g = -\frac{\partial P}{\partial z}. \tag{4.4}$$

where ρ_0 is the reference density, P the pressure, K_M the vertical eddy viscosity and g the gravity.

The pressure at depth z obtained by integrating equation 4.4:

$$P = P_{atm} + g\rho_0\eta + g\int_z^0 \rho\left(\acute{z}\right) d\acute{z}. \tag{4.5}$$

where P_{atm} is the atmospheric pressure and η the surface elevation.

The conservation equations for temperature and salinity:

$$\frac{\partial T}{\partial t} + U\frac{\partial T}{\partial x} + W\frac{\partial T}{\partial z} = \frac{\partial}{\partial z}\left(K_H \frac{\partial T}{\partial z}\right) + F_T, \tag{4.6}$$

$$\frac{\partial S}{\partial t} + U\frac{\partial S}{\partial x} + W\frac{\partial S}{\partial z} = \frac{\partial}{\partial z}\left(K_H \frac{\partial S}{\partial z}\right) + F_S. \tag{4.7}$$

where T is the temperature, S the salinity and K_H is the vertical eddy diffusivity.

The density is computed from an equation of state:

$$\rho = \rho\left(T, S\right). \tag{4.8}$$

taken from Gill (1982).

The horizontal eddy viscosity and diffusivity terms F_x, F_T and F_S:

$$F_x = \frac{\partial}{\partial x}\left(A_M \frac{\partial U}{\partial x}\right), \tag{4.9}$$

$$F_{T,S} = \frac{\partial}{\partial x}\left(A_H \frac{\partial\left(T, S\right)}{\partial x}\right). \tag{4.10}$$

where A_M is the horizontal eddy viscosity and A_H is the horizontal eddy diffusivity.

To close the set of equations, K_M, K_H, A_M and A_H must be computed. The horizontal viscosity, A_M, and the horizontal diffusivity, A_H, can be computed according to Smagorinsky (1963), or chosen to be constant in time and space. The vertical viscosity, K_M, and the vertical diffusivity, K_H, can be computed according to the Mellor & Yamada (1982) 2 1/2 level model or chosen to be constant in time and space.

In this study the horizontal viscosity, A_M, and the horizontal diffusivity, A_H, was chosen to be constant whereas the vertical viscosity, K_M, and the vertical diffusivity, K_H, was computed according to the Mellor & Yamada (1982) 2 1/2 level model. The values used are given in table 4.1.

Variable	Model setup 1	Model setup 2
A_M	100	10
A_H	0	0
$K_M(min)$	$1 \cdot 10^{-4}$	$1 \cdot 10^{-4}$
$K_M(max)$	1	1
$K_H(min)$	$1 \cdot 10^{-7}$	$1 \cdot 10^{-7}$
$K_H(max)$	1	1

Table 4.1: *Horizontal diffusivities, vertical viscosities and vertical diffusivities used in the two model setups.*

4.2 Boundary conditions

The model has a free surface where $z = \eta(x)$. There are no volume fluxes through the side walls where free slip conditions for the flow are applied. There are no advective or diffusive heat or salt fluxes on the side walls or at the bottom of the basin.

At the free surface motion is induced by an oscillating wind forcing. The equations for the wind field and the surface drag are given under the model setup section, as well as the equations for the bottom drag.

4.3 The σ-coordinate system

The equations are transformed into a bottom following σ-coordinate system. The variables (x, z, t) are transformed into (x^*, σ, t^*), where

$$x^* = x \qquad \sigma = \frac{z - \eta}{H + \eta} \qquad t^* = t. \tag{4.11}$$

σ ranges from $\sigma = 0$ at $z = \eta$ to $\sigma = -1$ at $z = -H(x)$.

4.4 The model setup

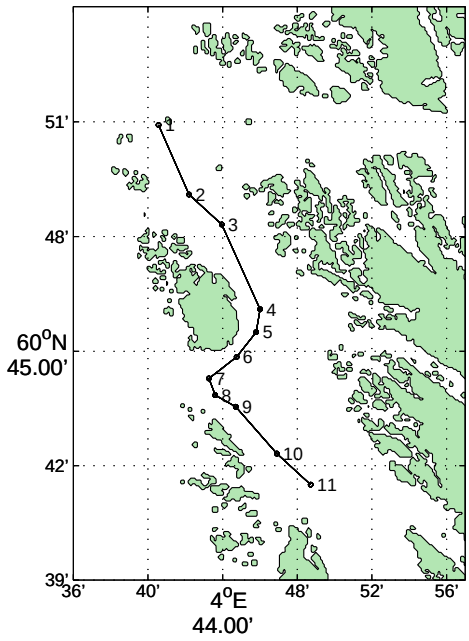

Figure 4.1: *Map over the Hjeltefjord with the model section marked in. The numbers marking the direction the plume of intruding dense water follows.*

The 2D BOM model, using the (x, z, t) coordinate system, was applied. The model section is shown in Figure 4.1. It is chosen to follow the deepest part of the fjord. The topography was set up using a sea map to find the depths along the section. It was smoothened with a Shapiro filter (Shapiro 1970).

Two different model domains with different resolution, density stratification and wind forcing was used to study a plume of water progressing through the deep channel in Hjeltefjorden.

4.4.1 Setup 1

The first model domain was $0 \leq x \leq L_x$ with $L_x = 31.5km$. There was a vertical closed boundary at $x = L_x$. At $x = 0$ there was an open boundary. The domain was discretized by a grid of 120×31 points giving av horizontal grid spacing of $265m$. The 2D courant number was $C_0 = \frac{\Delta t \cdot |u|}{\Delta x} = 0.16$. C_0 must be less than 1, $C_0 < 1$, to resolve the physics of waves at lengthscale $2\Delta x$.

The density stratification was set up according to CTD-measurements from a similar fjord, with densities ranging between $1024.5kgm^{-3}$ and $1027.3kgm^{-3}$. The following

figure is a cross-section of the model domain. It shows the initial density stratification as well as the topography of the deep channel in Hjeltefjorden.

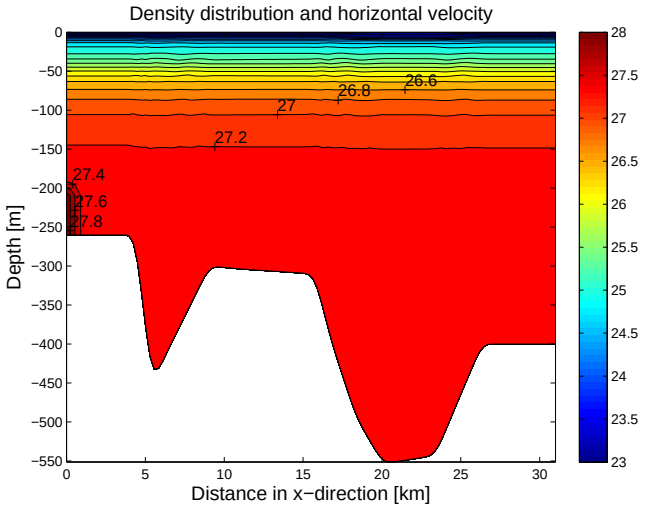

Figure 4.2: *Initial density stratification*

Motion was induced by an oscilllating wind forcing. The wind speed in x-direction at time t was

$$W_x = W_{max} \times \sin(\omega t), \tag{4.12}$$

where W_{max} was the maximum wind speed in ms^{-1} $10m$ above the sea surface and ω the frequency of the wind oscillation. In this study W_{max} was $10ms^{-1}$. The wind increased from zero over a period of 12 hours. From the wind speed the drag was computed, see Large & Pond (1981),

$$\tau_x = \frac{1.3}{1024.5} c_d W_{max} W_x, \tag{4.13}$$

where

$$c_d = \begin{cases} 1.14 \times 10^{-3} & \text{if } 4ms^{-1} < W_{max} \leq 10ms^{-1} \\ (0.49 + 0.065W_{max}) \times 10^{-3} & \text{if } 10ms^{-1} < W_{max} < 26ms^{-1}. \end{cases}$$

The bottom stress was given by

$$\tau_{bx} = \rho_0 C_D |U_b| U_b \tag{4.14}$$

where the drag coefficient C_D was given by

$$C_D = max\left[0.0025, \frac{\kappa^2}{(\ln(z_b/z_0))^2}\right] \tag{4.15}$$

and z_b was the distance from the nearest grid point to the bottom. $\kappa = 0.4$ was the Von Karman constant. $z_0 = 0.01m$ was the bottom roughness parameter, see Weatherly & Martin (1978).

When defining the model area, the topography, and the density stratification, the boundaries were kept closed. Also when the wind field was introduced, the boundaries were closed so that the effects could be monitored. When everything seemed to be working properly, the northern boundary was opened. That was the place for inflow of Atlantic water. The southern boundary remained closed.

The incoming Alantic water was given the density $1028kgm^{-3}$ which was heavier than the residing deep water in the fjord. This density corresponded with measurements from the bottom of the Hjeltefjord at times with renewal of deep water.

Initially $U = W = 0ms^{-1}$ and $\eta = 0m$. A seven grid cell relaxation zone was added at the inflow of the fjord (Martinsen & Engedahl 1987). At each time step the velocity in this zone was updated according to

$$U = (1 - \alpha)\, U_{int} + \alpha U_{ext}, \tag{4.16}$$

where U_{int} was the unrelaxed values computed by the model and U_{ext} was a specified external value. The relaxation parameter α varied from 0 at $x = 0$ to 1 at the end of the zone.

Approximations to U_{ext} was computed for each timestep from approximations to U in the interior model domain,

$$U_{ext} = \frac{1}{L} \int_x^{x+L} U dx \tag{4.17}$$

and applied as the external boundary value for U. $L = 2 \times LB = 2 \times 220.5m = 441m$ was twice the length of the relaxation zone and $x = LB = 220.5m$. $LB = 7 \times 31.5m = 220.5m$ was the length of the seven grid relaxation zone.

The density was updated in a similar way

$$\rho = (1 - \alpha)\, \rho_{int} + \alpha \rho_{ext}, \tag{4.18}$$

$$\rho_{ext} = \frac{1}{L} \int_x^{x+L} \rho dx \tag{4.19}$$

$$\rho\,(z_M) = \begin{cases} \rho_{AW} & \text{if } U_{ext} > 0 \text{ for } -H < z < z_M < -200 \\ \rho & \text{otherwise,} \end{cases}$$

where $\rho_{AW} = 1028kgm^{-3}$, ρ was an approximation to ρ in the interior model domain and z_M was the depth at which the density was updated. $L = 441m$ was twice the length of the relaxation zone and $x = 220.5m$.

4.4.2 Setup 2

The second model domain was $0 \leq x \leq L_x$ with $L_x = 26.2km$. At $x = 0$ and at $x = L_x$ there were open boundaries. The domain was discretized by a grid of 1000×100 points giving av horizontal grid spacing of $26.2m$. The 2D courant number was 0.13.

The density stratification was set up using CTD-data from a cruise in Hjeltefjorden with M/S Haakon Mosby the 14th of October 1998. The CTD-profile from October (fig.4.4) was a typical summer profile, but was still used as this was the only CTD-measurements from Hjeltefjorden we could obtain. The CTD-profile used was taken further south than the locations of the current meters, and is marked in on the map in figure 4.3.

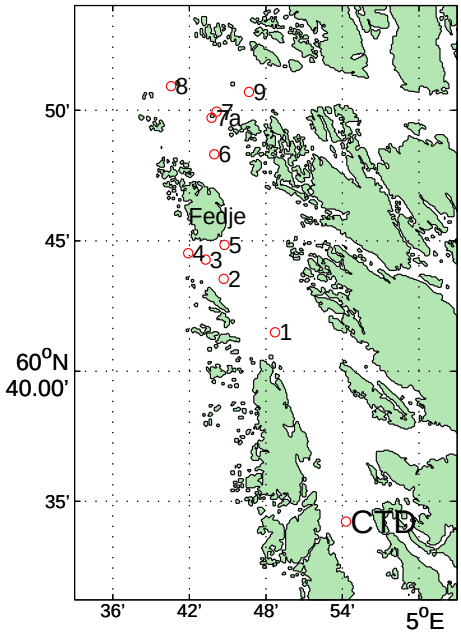

Figure 4.3: *Map over Hjeltefjorden with the location the CTD profile was taken as well as the locations of the current meters.*

.

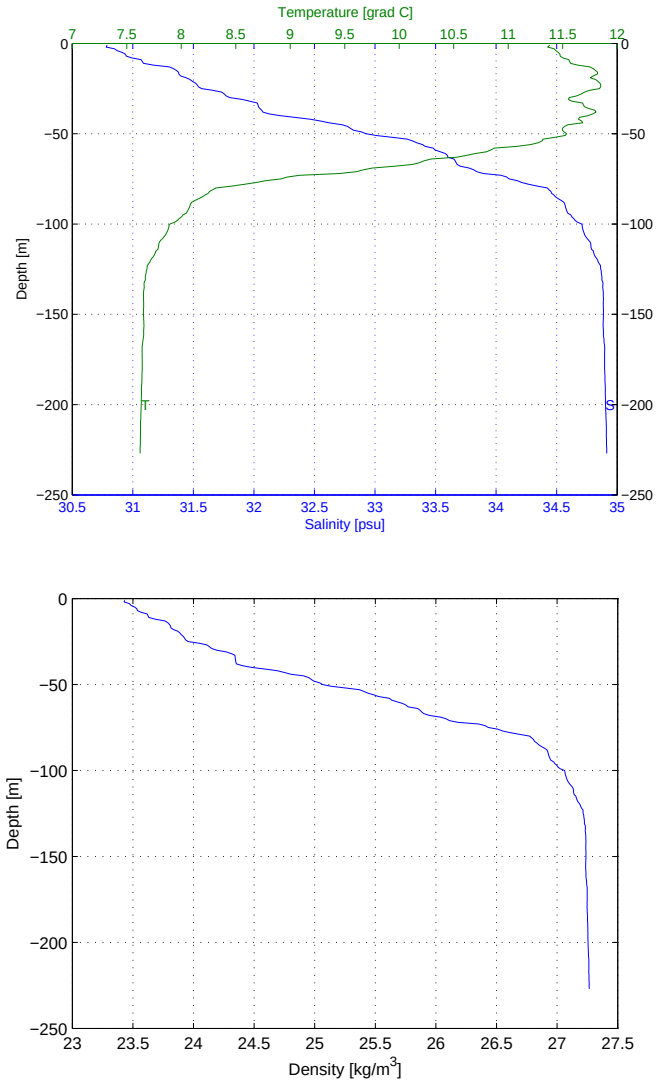

Figure 4.4: *Measured salinity, temperature and density from a CTD-profile taken in Hjeltefjorden at* $60°33'N$ *and* $4°54'E$ *the 14th of October 1998.*

The CTD-profile (fig.4.4) is showing a typical two-layer system. The upper layer is warm and fresh, whereas the lower layer is cold and salty. The profiles show a highly stratified upper layer and a well mixed lower layer. These profiles show that for Hjeltefjorden the density is most dependent on salinity. They have almost identical profiles.

The following figure is a cross-section of the model domain. It shows the initial density stratification set up using the CTD-data from Hjeltefjorden, as well as the topography of the deep channel in Hjeltefjorden. The density ranges from $1023.2kgm^{-3}$ to $1027.3kgm^{-3}$.

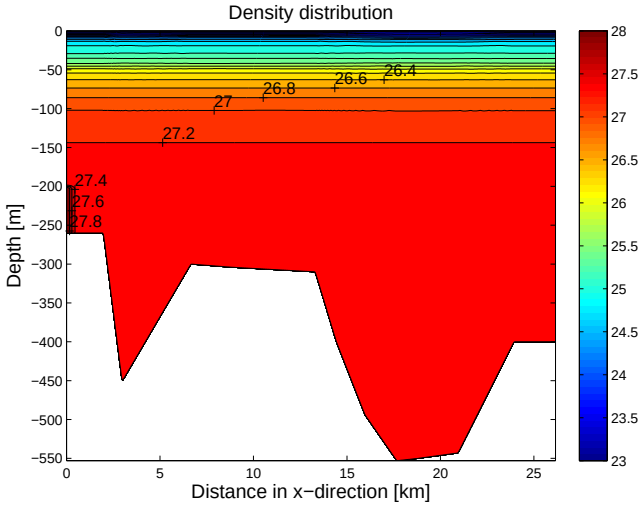

Figure 4.5: *Initial density stratification*

Motion was induced by a wind forcing. The wind field was set up using the time series of wind data from the station at the island of Fedje in Hjeltefjorden. (See chapter 2, Atmospheric data). The wind drag and bottom stress was computed similarly as in setup 1. The incoming Atlantic water was given the density $1028 kgm^{-3}$ as in setup 1.

Initially $U = W = 0ms^{-1}$ and $\eta = 0m$. A relaxation zone over 28 grid cells was added at the inflow of the fjord. At each time step the velocity in this zone was updated according to

$$U = (1 - \alpha)\, U_{int} + \alpha U_{ext}, \tag{4.20}$$

where U_{int} was the unrelaxed values computed by the model and U_{ext} was a specified external value. The relaxation parameter α varied from 0 at $x = 0$ to 1 at the end of the zone.

Approximations to U_{ext} was computed for each timestep

$$U_{ext} = \frac{1}{L} \int_{x}^{x+L} U dx \tag{4.21}$$

from approximations to U in the interior model domain, and applied as the external boundary value for U. $L = 2 \times LB = 2 \times 733.6m = 1467.2m$ was twice the length of the relaxation zone and $x = LB = 733.6m$. $LB = 28 \times 26.2m = 733.6m$ was the length of the 28 grid relaxation zone. The density was updated in a similar way

$$\rho = (1 - \alpha)\, \rho_{int} + \alpha \rho_{ext}, \tag{4.22}$$

$$\rho\,(z_M) = \begin{cases} \rho_{AW} & \text{if } U_{ext} > 0 \text{ for } -H < z < z_M < -200 \\ \rho & \text{otherwise,} \end{cases}$$

where $\rho_{AW} = 1028 kgm^{-3}$, ρ was an approximation to ρ in the interior model domain and z_M was the depth at which the density was updated.

After testing the model and concluding that it produced plausible values, the southern boundary was opened as well. That is the place for outflow of fjord water. The same prosedure was followed at the southern boundary. A 28 grid cell relaxation zone was added at the outflow of the fjord. The velocity in this zone was updated similarily as in the northern boundary zone.

$$U = (1 - \alpha) U_{int} + \alpha U_{ext}, \tag{4.23}$$

where U_{int} was the unrelaxed values computed by the model and U_{ext} was a specified external value. The relaxation parameter α varied from 0 at $x = L_x$ to 1 at the end of the zone.

Approximations to U_{ext} was computed for each timestep

$$U_{ext} = \frac{1}{L} \int_x^{x+L} U dx \tag{4.24}$$

from approximations to U in the interior model domain, and applied as the external boundary value for U. $L = 1467.2m$ was twice the length of the relaxation zone, and $x = L_x - L = 24.0km$. The density was updated in a similar way

$$\rho = (1 - \alpha) \rho_{int} + \alpha \rho_{ext}, \tag{4.25}$$

For each time step approximations to ρ_{ext}

$$\rho_{ext} = \frac{1}{L} \int_x^{x+L} \rho dx \tag{4.26}$$

were computed from approximations to ρ in the interior model domain, and applied as the external boundary values for ρ. $L = 1467.2m$ was twice the length of the relaxation zone, and $x = L_x - L = 24.0km$.

Results from the two model experiments will be given in the next chapter.

Chapter 5

Model results

The results from the two different model runs will be shown in this chapter. That will include density stratification, horizontal velocity and phase velocity of the plume of dense water progressing through Hjeltefjorden.

The purpose of the model runs is to represent a plume of dense water that intrudes the fjord basin. We will follow the plume as it decends down the slope of the sill and follows the bottom of the deep channel in the basin, lifting the residing bottom water to higher levels.

5.1 Setup 1

We see how a plume of dense Atlantic water moves into the fjord basin (fig.5.1). Because the plume is denser than the residing deep water in the fjord, it will follow the bottom of the fjord basin and replace the old basin water by lifting it to a higher level. The dense Atlantic water then starts mixing with the residing deep water in the fjord. The experiment shows that the pure Atlantic water with density $1028 kgm^{-3}$ is only present at the boundery where it is constantly refilled. Inside the fjord mixing lowers the density.

It takes the plume about 24 hours to reach the southern boundary of the fjord, which is closed. There the plume will be reflected and it will turn back. As time proceedes the basin will be filled up with dense Atlantic water. The effect is represented in the upper layers of the fjord where you can see a wave progressing into the fjord, be reflected, and returning out again.

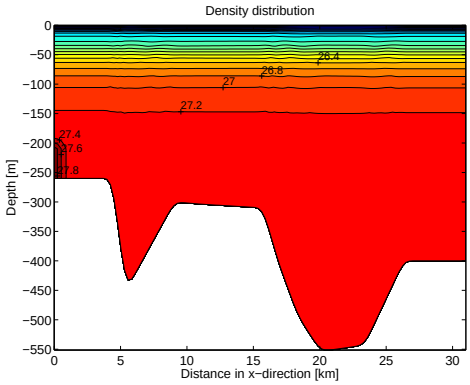

0h

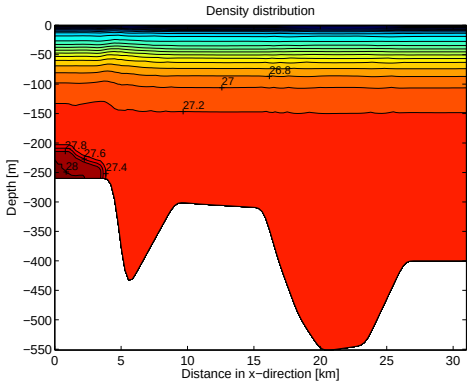

2h

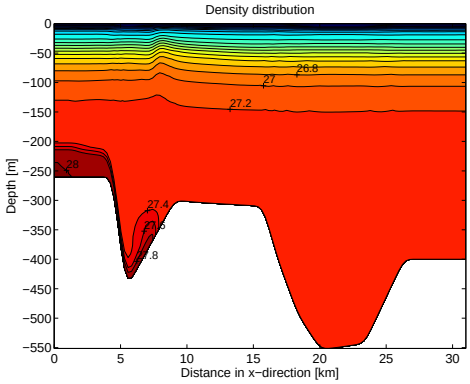

4h

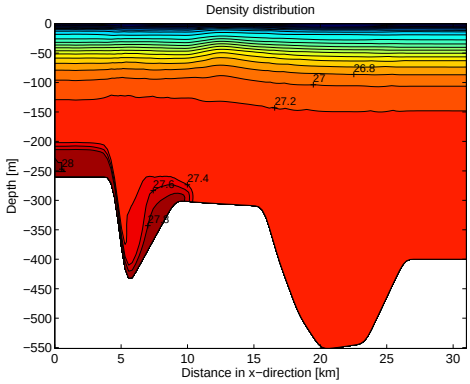

6h

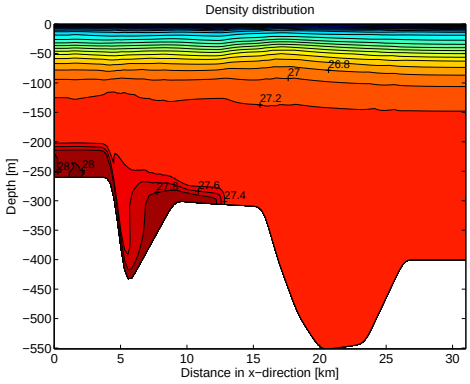

8h

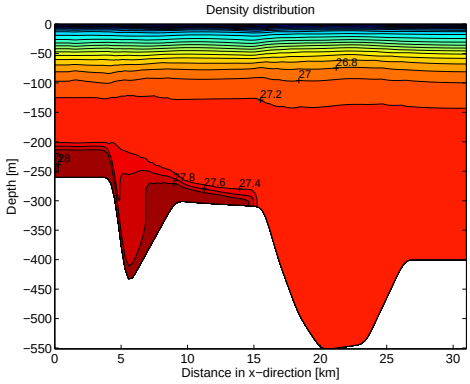

10h

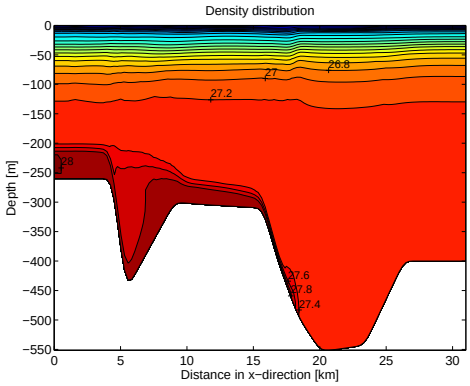

12h

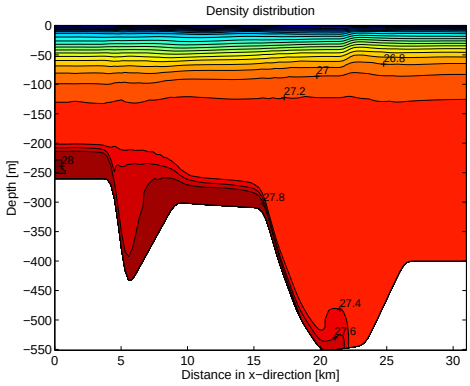

14h

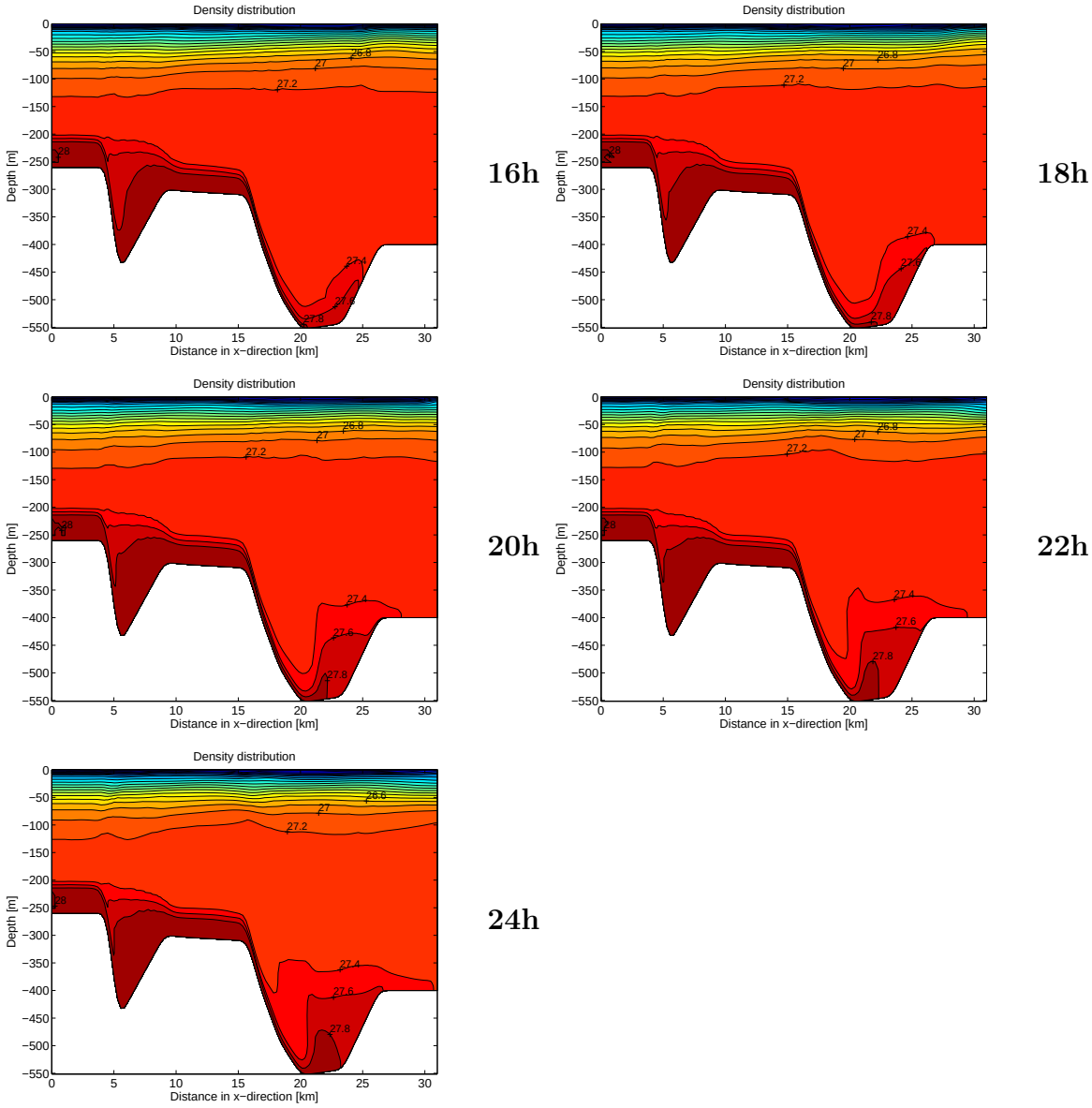

Figure 5.1: *The density stratification evolving with time from from the boundary was opened and 24 hours into the model run. Each plot is seperated by 2 hours in time. Note the deep dense plume propagating from left to right.*

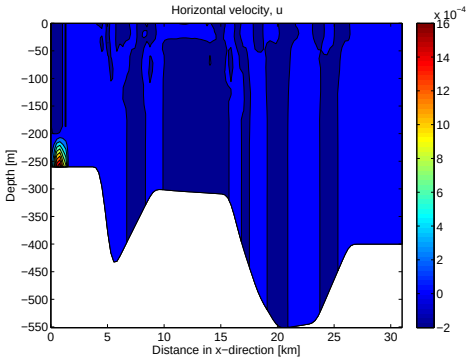

0h

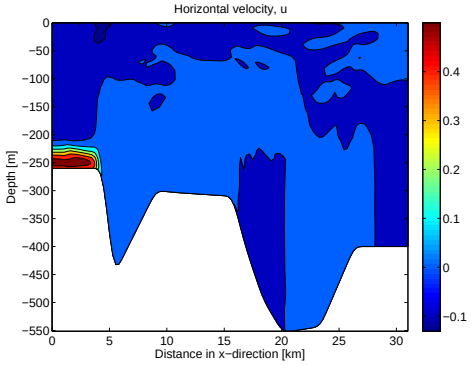

2h

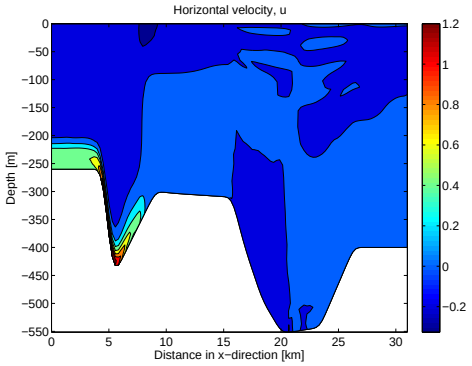

4h

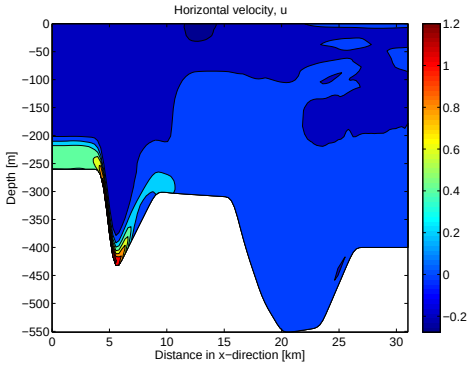

6h

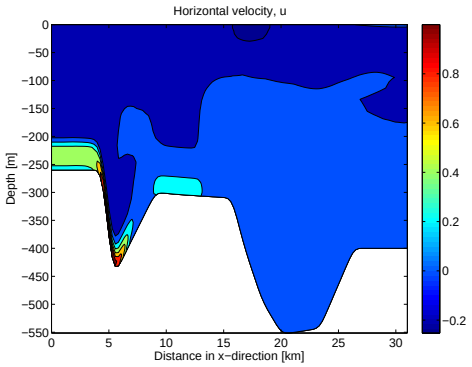

8h

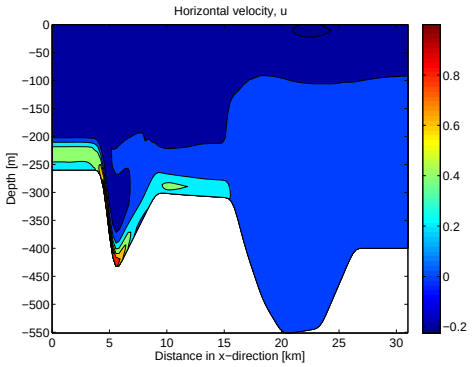

10h

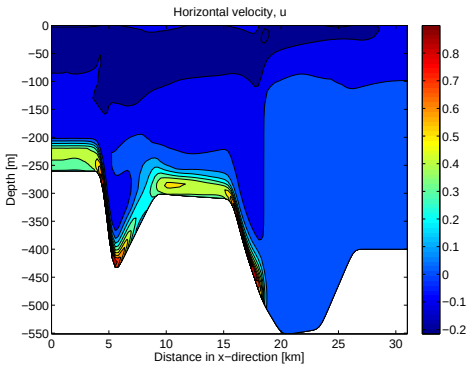

12h

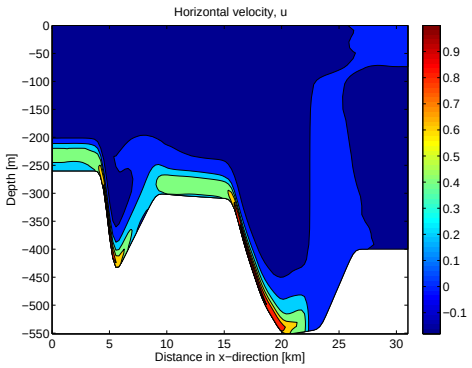

14h

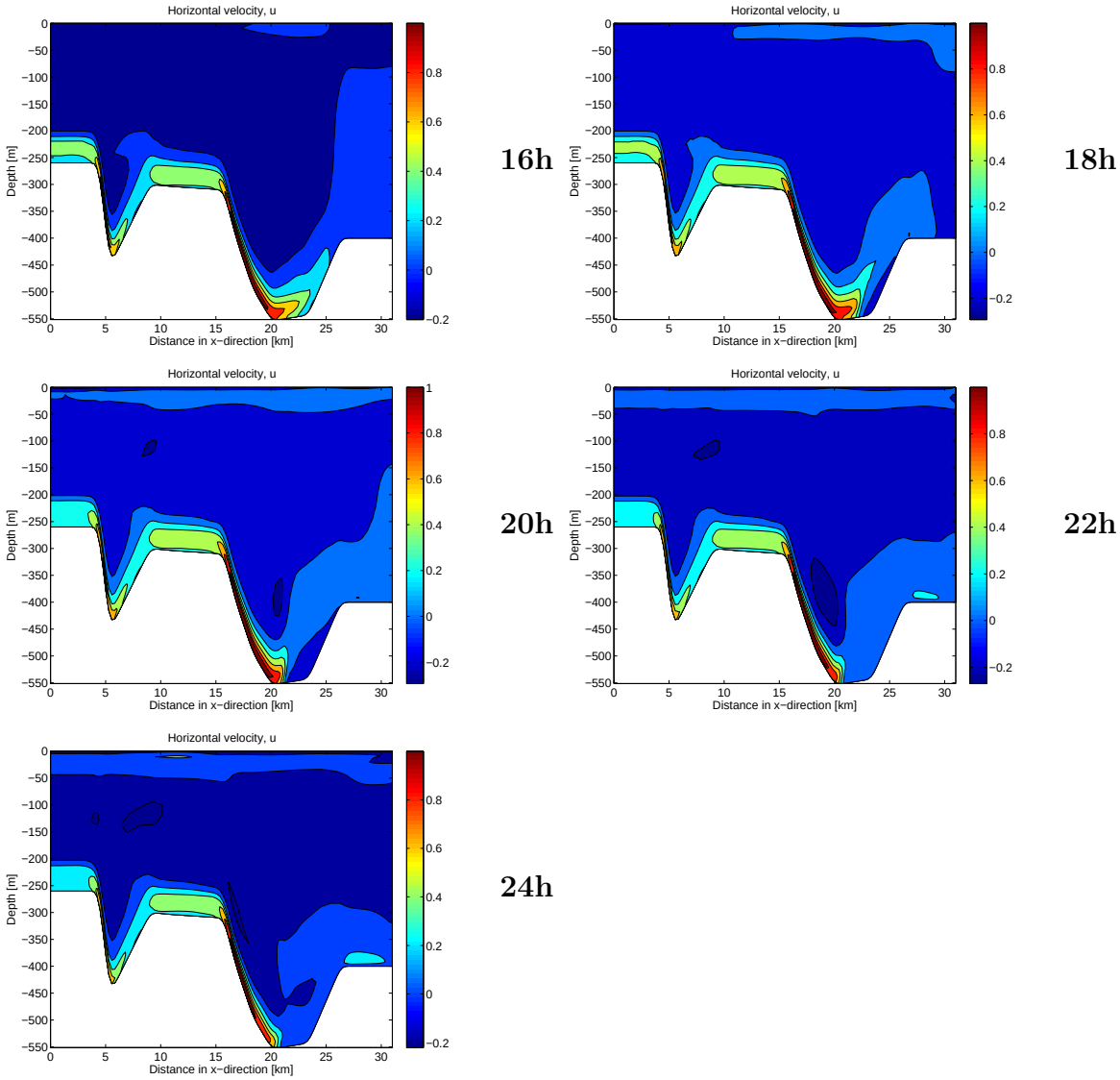

Figure 5.2: *The horizontal velocity evolving with time from the boundary was opened and 24 hours into the model run. Each plot is seperated by 2 hours in time. Note the deep dense plume propagating from left to right.*

The wind field makes water pile up at the northern boundary which creates a pressure gradient headed into the fjord. This gradient drives the denser Atlantic water into the fjord and it follows the bottom of the fjord basin and replaces the residing deep water.

The figure shows the horizontal velocity of the plume moving into the fjord basin. Down the basin slopes the velocity is high, where it is flat and up the slopes the velocity is lower.

5.2 Setup 2

The plume of dense Atlantic water progresses through the fjord basin in a similar manner in setup 2 as in setup 1. The main difference is the velocity of the plume. Whereas in setup 1 the plume reached the southern boarder in 24 hours, the plume reached the southern boarder in 12 hours in setup 2. The progression of the plume is also clearly represented in the upper layers of the fjord. You can see a disturbance travelling through the fjord in the same velocity as the plume, as a progressive wave.

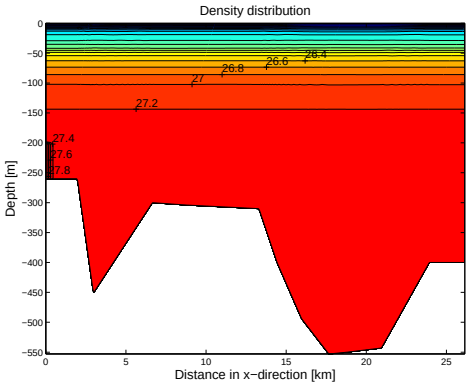

0h

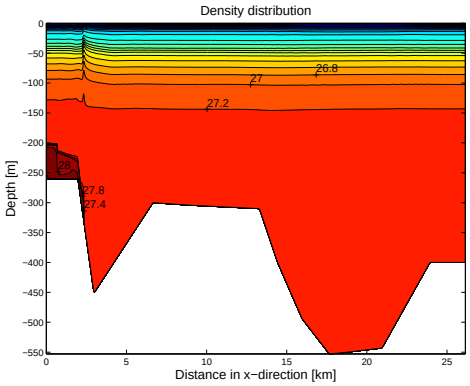

1h

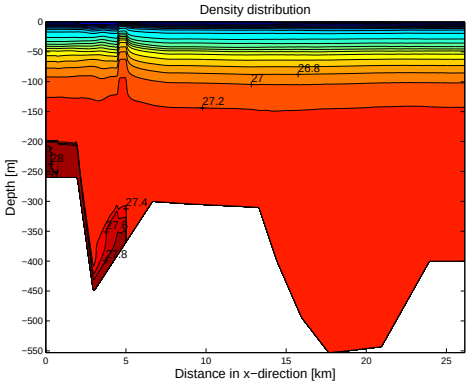

2h

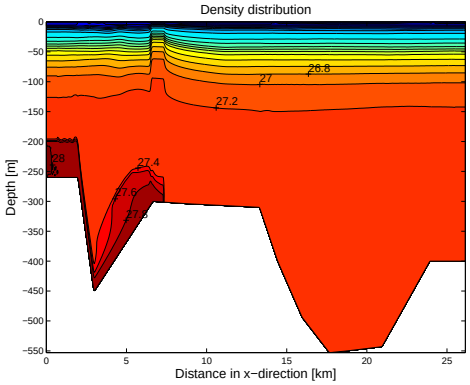

3h

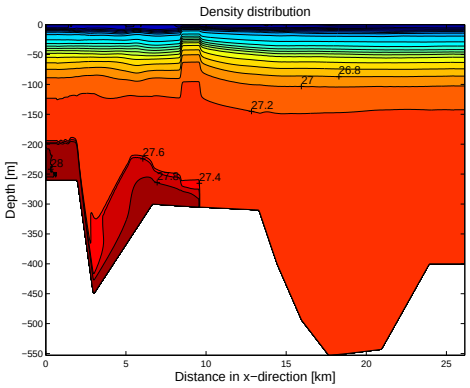

4h

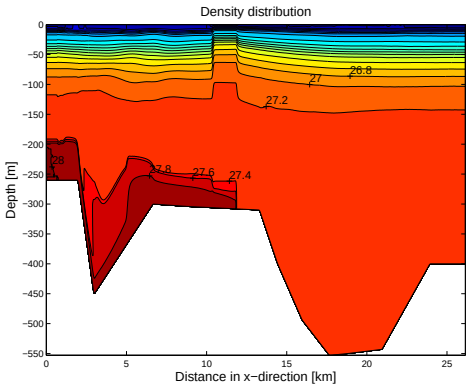

5h

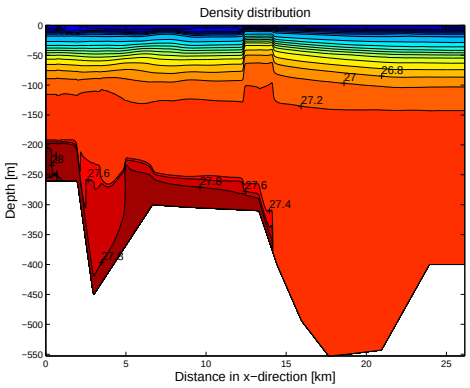

6h

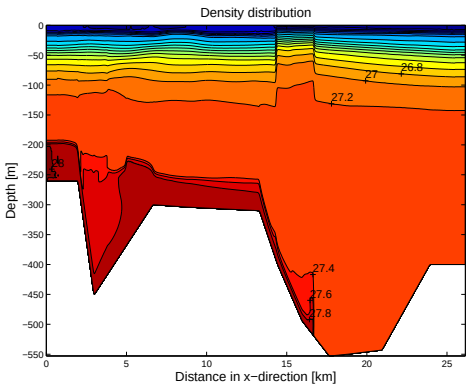

7h

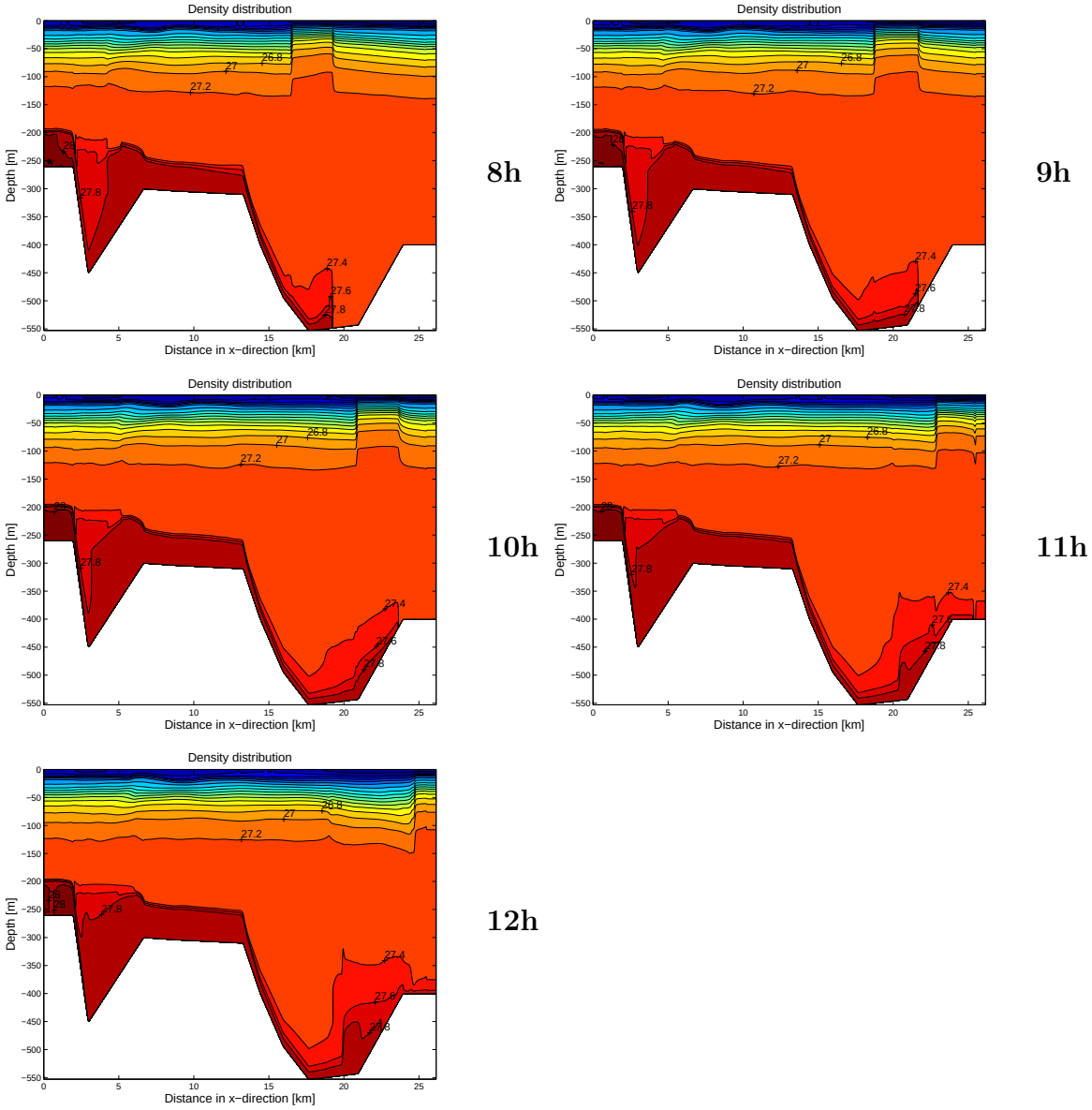

Figure 5.3: *The density stratification evolving with time from the boundary was opened and 12 hours into the model run. Each plot is seperated by 1 hour in time. Note the deep dense plume propagating from left to right.*

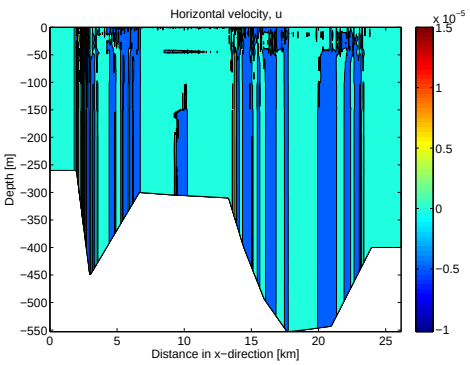

0h

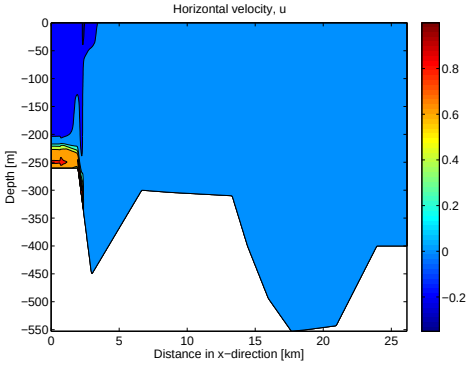

1h

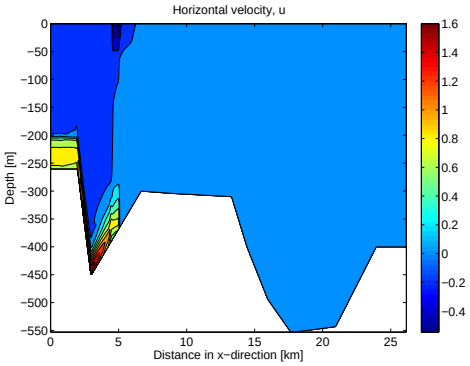

2h

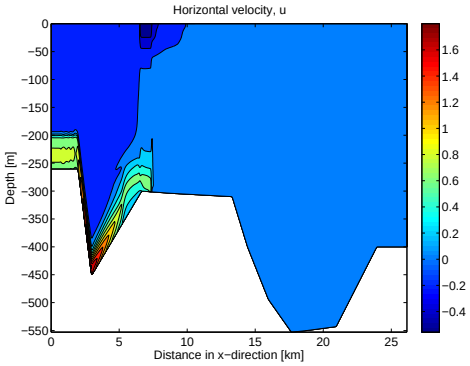

3h

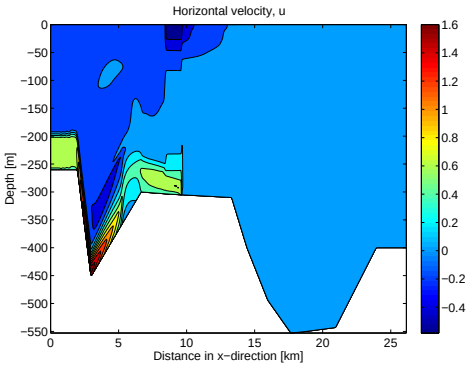

4h

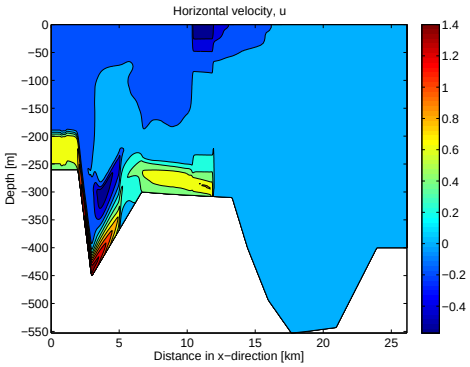

5h

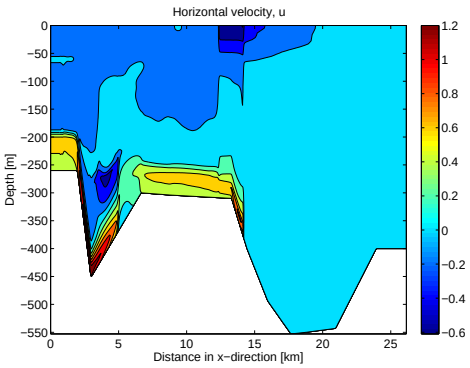

6h

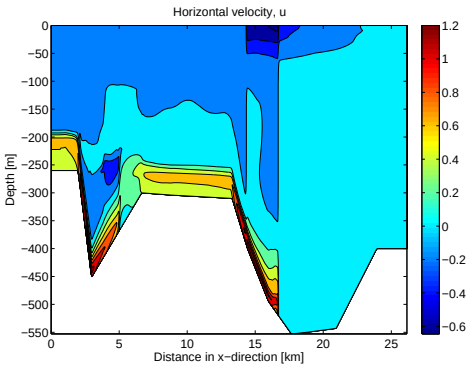

7h

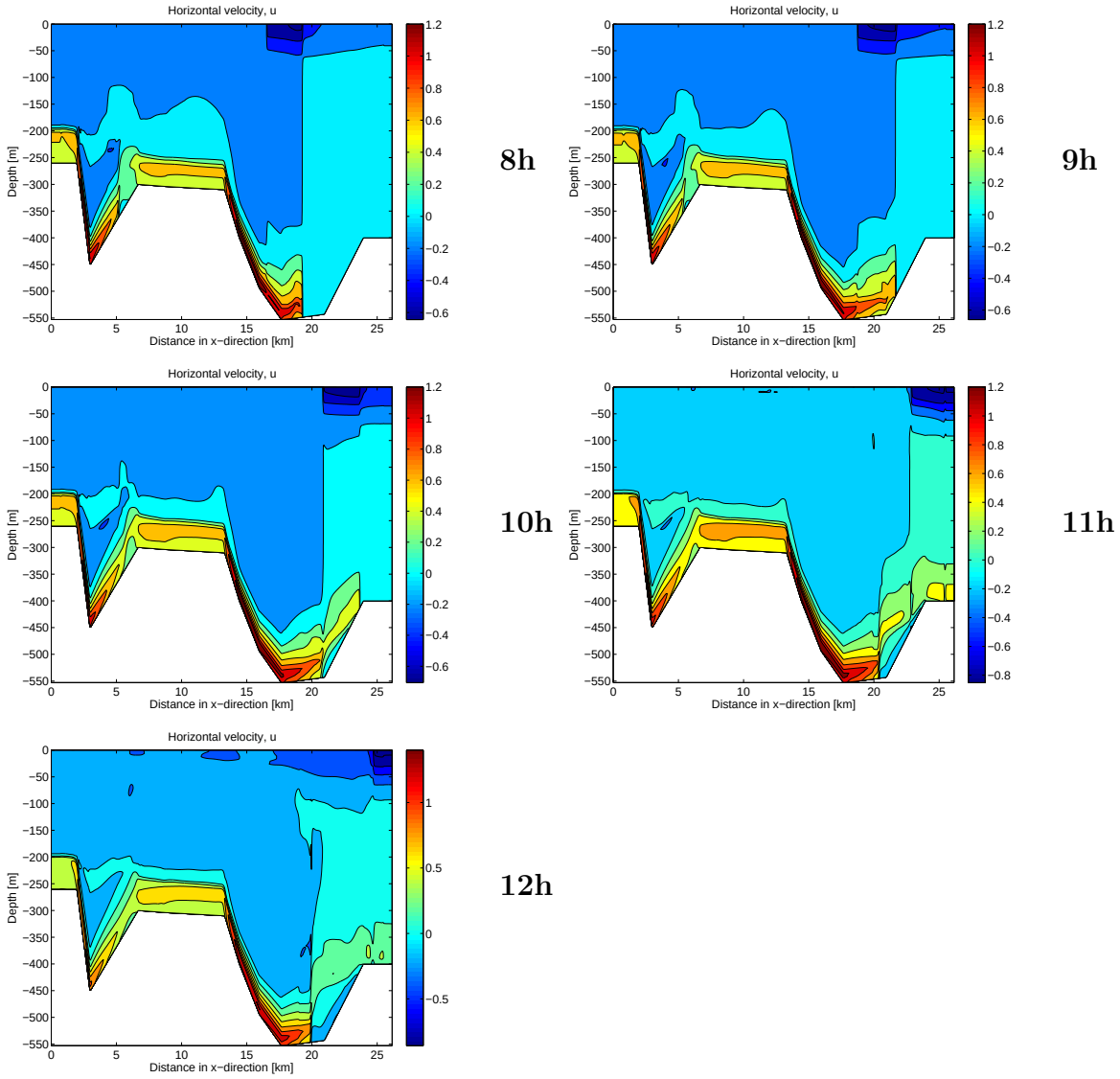

Figure 5.4: *The horizontal velocity evolving with time from the boundary was opened and 12 hour into the model run. Each plot is seperated by 1 hour in time. Note the deep dense plume propagating from left to right.*

In setup 2 the plume of dense Atlantic water progresses through the fjord faster than in setup 1. As the plume progresses through the fjord basin, a counter-current is set up in the upper layer. The counter-current follows the plume throughout the length of the basin. After 4 hours a counter-current is set up directly above the plume heading up the first slope.

Chapter 6

Discussion

A discussion of the results from the numerical model will be shown in this chapter. Afterwards a comparison between the observational data and the numerical model results will be made.

6.1 Setup 1

When the denser water is moving into the fjord basin, it moves with different velocities corresponding to the slope of the topography and the difference in density between the moving plume of water and the surrounding water.

The Froude number, F_r, is used to describe the flow pattern over an obstacle.
$F_r > 1$: the flow is super-critical, the current is strong and shallow.
$F_r < 1$: the flow is sub-critical, the current is weaker and thicker.

$$F_r = \frac{U}{\sqrt{g'H}} \tag{6.1}$$

where U is the velocity of the plume, g' the reduced gravity and H the height of the obstacle. From figure 5.1 and 5.2 we get approximate numbers for $U = 0.5m/s$, $H = 50m$ and $g' = \frac{\Delta\rho}{\rho} \times g = \frac{0.6}{1027.8} \times 9.8m/s^2$.

$$F_r = 1 \tag{6.2}$$

The Froude number gives that down the first slope the movement is critical, and there is almost no mixing between the plume and the surrounding water. At the bottom, and at the top of the slopes, the plume moves slower and we get vigorous mixing with the surrounding water.

From the density distribution figure one can see that the dense Atlantic water mixes with the residing deep water in the fjord soon after entering the basin. Since the southern boundary is closed, the incoming water is trapped in the basin, and as time

proceeds the basin is filled up with a mix between the dense Atlantic water, and the residing deep water from the fjord.

One can see the influence of the incoming dense water in the upper density layers. The disturbance is felt throughout the water column and the effect carries through the whole length of the basin. The upper layers are bent upwards as the plume of dense water is progressing into the fjord basin. The upper density layers moves along the fjord basin like a progressive wave. It is reflected at the southern boundary and turns back towards the northern boundary.

The velocity of the front of the plume, the propagation velocity, can be determined by looking at the the movement of the lower layer. By plotting along-bottom density as a function of time the velocity can be determined.

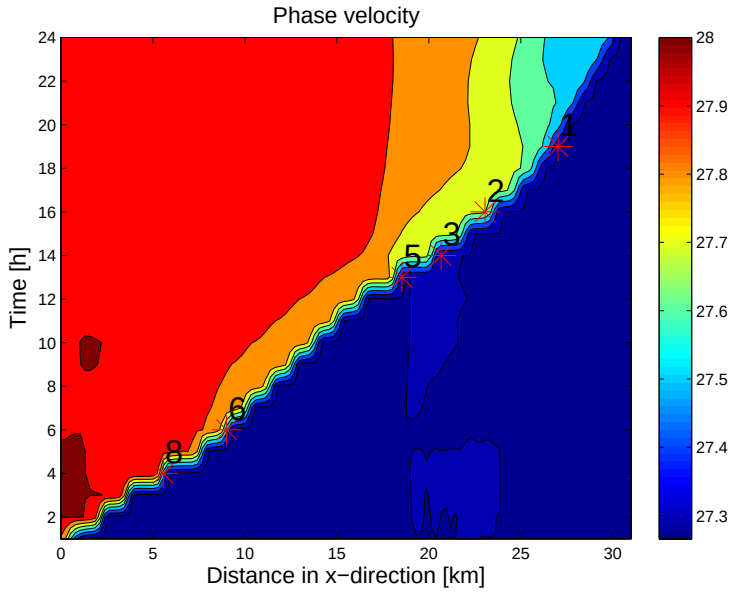

Figure 6.1: *Along-bottom density as a function of time, for setup 1. The stations are marked in with red stars.*

Figure 6.1 and eq. 2.1 gives the front velocity $c = 50cm/s$ at the northern end of the model section and $c = 20cm/s$ at the southern end of the model section. The plume is losing its velocity at the end of the fjord. The reason for this may be the closed boundary which creates a false obstacle that is not present in Hjeltefjorden.

6.2 Setup 2

When comparing model setup 1 and 2, the two most important differences between the two are the resolution and the boundaries. Setup 2 has a much higher resolution with a horizontal grid spacing of $26.2m$ compared to the horizontal grid spacing of $265m$ from setup 1. Furthermore, in setup 2 the southern boundary in the model section is open, whereas in setup 1 it is closed.

The open boundary in setup 2 generates higher velocities in model run 2 than in model run 1. The reason for this is that the open boundary creates a pull on the plume that is not present with a closed boundary. For the same reason the volume transport in model run 2 is bigger than in model run 1. This creates more mixing between the plume of dense water and the surrounding water. But down the first slope there is almost no mixing. From figure 5.3 and 5.4 we get approximate numbers for $U = 0.5m/s$, H and g' are the same as in setup 1. We can now calculate the Froude number:

$$F_r = 2 \tag{6.3}$$

The Froude number gives that the movement is super-critical down the first slope, which explaines why there is alomost no mixing between the plume and the surrounding water.

After 4 hours a counter current is set up directly above the plume heading up the first slope (fig.5.4). Because of the steep slope the plume is slowed down and starts mixing with the surrounding water. Some of the plume water that is mixed with the surrounding water falls back down the slope and creates the small counter-current above the plume. The counter-current disaperars about 8 hour into the model run.

Model setup 2 was run non-hydrostatic as well as hydrostatic. The hope was to see more of the dynamics in the plume especially realted to overflows down the slopes. But the results from the non-hydrostatic run was similar to the results from the hydrostatic run and gave no more information about the dynamics of the plume. The reason for this may be that the resolution was not high enough.

The velocity of the front of the plume, the propagation velocity, can be determined by looking at the the movement of the lower layer. By plotting along-bottom density as a function of time the velocity can be determined.

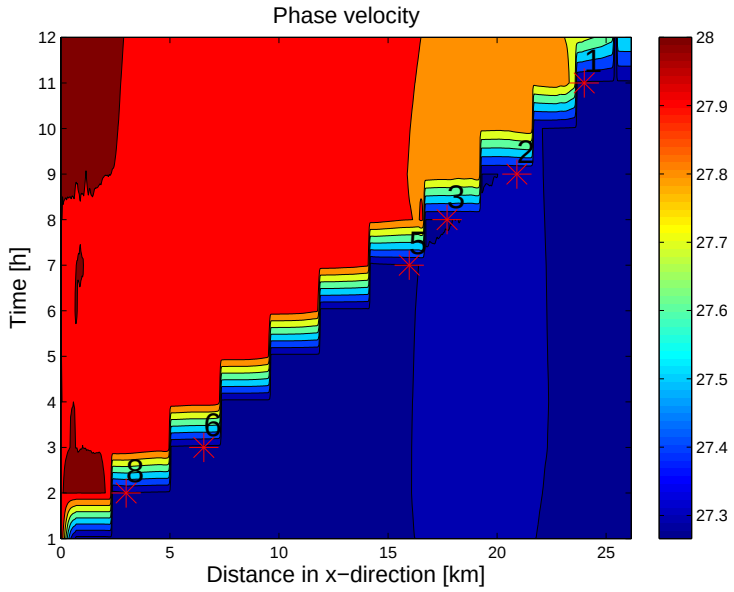

Figure 6.2: *Along-bottom density as a function of time, for setup 2. The stations are marked in with red stars.*

Figure 6.2 and eq. 2.1 gives the front velocity $c = 65cm/s$ throughout the model section. The front velocity of the plume in model run 2 is not reduced at the end of the fjord as in model run 1. This is probably because of the open boundary at the south end of the fjord. The larger volume transport in the plume of dense water in model run 2 compared to model run 1 may be the reason for the larger front velocity.

6.3 Observational data versus model results

To compare the observational data with the numerical model results, we will look into the front velocities of the plumes of dense water progressing through Hjeltefjorden.

Model Setup 1			
Location	Period	Observed velocity of the plume	Modeled velocity of the plume
station $8-6$	1	$12cm/s$	$50cm/s$
station $6-5$	1	$12cm/s$	$50cm/s$
station $5-3$	1	$15cm/s$	$50cm/s$
station $3-2$	1	$25cm/s$	$50cm/s$
station $2-1$	1	$53cm/s$	$20cm/s$
station $7a-6$	2	$16cm/s$	$50cm/s$
station $6-5$	2	$17cm/s$	$50cm/s$
station $5-3$	2	$26cm/s$	$20cm/s$

Table 6.1: *Observed front velocity of the plume of dense water progressing through Hjeltefjorden, compared with modeled front velocity from model setup 1.*

Model Setup 2			
Location	Period	Observed velocity of the plume	Modeled velocity of the plume
station $8-6$	1	$12cm/s$	$65cm/s$
station $6-5$	1	$12cm/s$	$65cm/s$
station $5-3$	1	$15cm/s$	$65cm/s$
station $3-2$	1	$25cm/s$	$65cm/s$
station $2-1$	1	$53cm/s$	$65cm/s$
station $7a-6$	2	$16cm/s$	$65cm/s$
station $6-5$	2	$17cm/s$	$65cm/s$
station $5-3$	2	$26.2cm/s$	$65cm/s$

Table 6.2: *Observed front velocity of the plume of dense water progressing through Hjeltefjorden, compared with modeled front velocity from model setup 2.*

The front velocities from model run 1 and 2 are of the same order of magnitude as the observed front velocities and is therefore comparable.

The front velocity from model run 1 (table 6.1) is closer to the observed front velocity than the front velocity from model run 2 (table 6.2). But because of the closed boundary in setup 1, the velocity of the plume decreases at the end of the model section.

Model run 1 gives the best results according to the magnitude of the front velocity, but fails at the southern end of the model section because of the closed boundary.

Chapter 7

Summary and conclusions

In this study, data obtained by $RCM-7$ current meters located in Hjeltefjorden, were analysed and compared to results from two different setups of a numerical σ-coordinate ocean model, Bergen Ocean Model (BOM). The observational data showed two very clear periods where the properties of the deep water in the fjord where altered in connection with bottom water renewal. The two setups of the numerical model were used to study how a plume of dense water progresses through the fjord basin in connection with bottom water renewal. Both setups produced good results which could be compared to the observational data.

Time series of observational wind data and NCEP reanalysis data were used to test the hypothesis that offshore surface Ekman transports, and compensating deep onshore flows lifting dense water over the sill, are causing bottom water renewal. The wind data showed northerly winds at the two periods of bottom water renewal. At the west coast of Norway northerly winds induce divergence in Ekman transports and upwelling of dense water, which can lead to bottom water renewal. The NCEP reanalysis data showed a low pressure system over Norway at the to periods of bottom water renewal. At the west coast of Norway these will cause northerly winds.

The questions posed in the introduction:

- Are periods of bottom water renewal recognizable in the observational data?
- What is the time needed to exchange the bottom water in Hjeltefjorden?
- Can periods of bottom water renewal be explained by atmospheric data?
- Can bottom water renewal be reproduced in a numerical model?
- How well do numerical model results compare to observational data?

The main findings are:

- During the measurement period of about half a year, two periods of bottom water renewal were especially clear. Period 1 in December 1998 and period 2 in February 1999. The intuding of new water masses was very clear in the temperature measurements. It was recorded a temperature drop of up to $0.5°C$ associated with a plume of Atlantic dense water progressing through the fjord basin. The intruding of Atlantic water was also appearent in the current measurements. A rise in the current velocity was evident at most of the measurement stations.

- From summarizing the propagation times in table 2.2 we find that the observed plume of dense water from period 1 uses about 40 hours from station 8 to station 1. This means that the bottom water in Hjeltefjorden is renewed in the course of 2 days. The reason why the exchange is this rapid, is the wide and deep mouth of Hjeltefjorden.

- Both the observed wind data from Fedje and the NCEP reanalysis data shows us that period 1 and 2 of bottom water renewal can be explained using atmospheric data. The observed wind data (fig.3.2) shows that the wind field shifts from from southerly to northerly at the days of bottom water renewal. Northerly winds at the west coast of Norway produces upwelling of dense water at the coast, which can lead to bottom water renewal in the fjords. The NCEP reanalysis data (fig.3.3 and fig.3.4) shows a low pressure system over Norway at the days of bottom water renewal. Low pressure systems over Norway are connected with northerly winds at the west coast of norway.

- Both the numerical model setups did well representing a plume of dense water progressing through Hjeltefjorden.

- The observational data and the numerical model results can be compared by looking at the front velocity of the plume. We found that the model setups produces somewhat larger velocities than the observational data gives us.

Bibliography

Arneborg, L., Erlandsson, C., Liljebladh, B. & Stigebrandt, A. (2004), 'The rate of inflow and mixing during deep-water renewal in a sill fjord', *Limnol. Oceanogr.* **49**, 768–777.

Berntsen, H., Kowalik, Z., Sælid, S. & Sørli, K. (1981), 'Efficient numerical simulation of ocean hydrodynamics by a splitting procedure', *Modeling, Identifaction and Control* **2**, 181–199.

Berntsen, J. (2000), USERS GUIDE for a modesplit σ-coordinate numerical ocean model, Technical Report 135, Dept. of Applied Mathematics, University of Bergen, Johs. Bruns gt.12, N-5008 Bergen, Norway. 48p.

Berntsen, J., Aksnes, D. & Foldvik, A. (2002), 'Production enhancement by artificial upwelling: a simulation study', *Hydrobiologia* **484**, 177–190.

Berntsen, J., Xing, J., Furnes, G. & Davies, A. (2003), 'Non-hydrostatic effects along shelf slopes and shelf edges'. Unpublished results.

Brown, E., Colling, A., Park, D., Phillips, J., Rothery, D. & Wright, J. (1995), *Seawater: Its Composition, Properties and Behaviour*, Open University, Walton Hall, Milton Keynes and Butterworth-Heinemann. ISBN-0-7506-3715-3.

Cannon, G. & Laird, N. (1980), Characteristics of flow over a sill during deep water renewal, *in* H. Freeland, D. Farmer & C. Levings, eds, 'Fjord oceanography', Plenum Press.

Eidnes, G. (1999), VESTPROSESS Current Measurements Summary Report, Technical report, SINTEF.

Fofonoff, P. & Millard, R. J. (1983), Unesco 1983. Algorithms for computation of fundamental properties of seawater, Technical Report 44. 53pp.

Gade, H. & Edwards, A. (1980), Deep water renewal in fjords, *in* H. Freeland, D. Farmer & C. Levings, eds, 'Fjord oceanography', Plenum Press.

Gill, A. E. (1982), *Atmosphere-Ocean Dynamics*, Academic Press, Inc. ISBN-0-12-283520-4.

Helle, H. (1978), Summer replacement of deep water in Byfjord, Western Norway: Mass exchange across the sill induced by coastal upwelling, *in* J. Nihoul, ed., 'Hydrodynamics of Estuaries and Fjords', Elsevier.

Large, W. & Pond, S. (1981), 'Open ocean momentum flux measurements in moderate to strong winds', *J. Phys. Oceanogr.* **11**, 324–336.

Liungman, O., Rydberg, L. & Göransson, C. (2001), 'Modeling and observations of deep water renewal and entrainment in a Swedish sill fjord', *J. Phys. Oceanogr.* **31**, 3401–3420.

Martinsen, E. & Engedahl, H. (1987), 'Implementation and testing of a lateral boundary scheme as an open boundary condition in a barotropic ocean model', *Coastal Engineering* **11**, 603–627.

Mellor, G. & Yamada, T. (1982), 'Development of a turbulence closure model for geophysical fluid problems', *Reviews of Geophysics and Space Physics* **20**, 851–875.

Mesinger, F. & Arakawa, A. (1976), 'Numerical Methods used in Atmospheric Models, Volume I'. WMO/ICSU Joint Organizing Committee, Garp Publication Series No. 17.

Molvær, J. (1980), Deep-water renewals in the Frierfjord - An Intermittently Anoxic Basin, *in* H. Freeland, D. Farmer & C. Levings, eds, 'Fjord oceanography', Plenum Press.

Shapiro, R. (1970), 'Smoothing, filtering and boundary effects', *Rev. Geophys. and Space Phys.* **8**, 359–387.

Smagorinsky, J. (1963), 'General circulation experiments with the primitive equations, I. The basic experiment', *Monthly Weather Review* **91**, 99–164.

Wallace, J. M. & Hobbs, P. (1977), *Atmospheric Sience an introductory survey*, Academic Press, Inc. ISBN-0-12-732950-1.

Weatherly, G. & Martin, P. (1978), 'On the structure and dynamics of the ocean bottom boundary', *J. Phys. Oceanogr.* **8**, 557–570.